

**Investigation of the Structural, Electrical and Magnetic
Properties of Mn-Doped AlFeO₃**

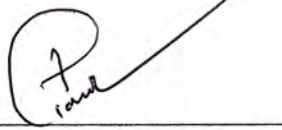


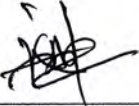

by
Tanzina Tabassum

MASTER OF SCIENCE IN PHYSICS

Department of Physics
BANGLADESH UNIVERSITY OF ENGINEERING AND TECHNOLOGY
February 2021

The thesis titled “Investigation of the Structural, Electrical and Magnetic Properties of Mn-Doped AlFeO₃” submitted by Tanzina Tabassum, Roll No.: 0417142508F, Session: April-2017, has been accepted as satisfactory in partial fulfillment of the requirement for the degree of Master of Science (M. Sc.) in Physics on 6 February, 2021.

BOARD OF EXAMINERS

1.  (_____)
Dr. Md. Feroz Alam Khan (Supervisor)
Professor, Department of Physics, BUET, Dhaka. Chairman
2.  (_____)
Dr. Md. Rafi Uddin
Professor and Head, Department of Physics,
BUET, Dhaka-1000. Member
(Ex-Officio)
3.  (_____)
Dr. Mohammed Abdul Basith
Professor, Department of Physics, BUET,
Dhaka-1000. Member
4.  (_____)
Dr. Mohammad Khurshed Alam
Associate Professor, Department of Physics, BUET,
Dhaka-1000. Member
5.  (_____)
Dr. Supriya Saha
Professor, Department of Physics,
University of Dhaka. (External)
Member

CANDIDATE'S DECLARATION

It is hereby declared that this thesis or any part of it has not been submitted elsewhere for the award of any degree or diploma.

Tanzina Tabassum

Tanzina Tabassum

Dedicated To
My
Beloved Parents

Acknowledgments

At first, I express all my admiration and devotion to the almighty Allah who has given me the strength and opportunity to complete this thesis work.

I express my gratitude and respect to my supervisor Prof. Dr. Md. Feroz Alam Khan, Department of Physics, Bangladesh University of Engineering and Technology (BUET), for his continuous guidance, supervision, support, motivation, and encouragement in my research work. I am very grateful to Dr. Md. Rafi Uddin, Professor & Head, Department of Physics, BUET, Dhaka, Bangladesh for his valuable suggestions and inspiration. I am also grateful to Dr. Mohammad Khurshed Alam for his continuous assistance during the research work. I would like to acknowledge all of my respected teachers of the Department of Physics, BUET for their cooperation and constructive suggestions in my research work.

I am so thankful to all of my fellow Laboratory co-researchers, especially Md. Ziaul Ahsan, Md. Shohel Rana, Tofayal Hossain Mollah, M. A. A. Bally, Md. Naved Iqbal, and Aminul Islam for their encouragement and suggestions. I am also thankful to the department of Glass & Ceramic Engineering (GCE), BUET for their cooperation and support throughout the research. I would like to extend my gratitude to all of my friends, youngers for their good wishes and cooperation throughout the study.

I would like to acknowledge BUET's authority for providing necessary permissions and financial support for this research work and BUET central library for their valuable information service. The International Science Program (ISP), Uppsala University, Sweden, is thankfully acknowledged for its technical assistance.

Finally, I am grateful to my lovely mother, father, and sisters for their moral support and inspiration.

(Tanzina Tabassum)

Author

ABSTRACT

Combining different physical properties into one material is promising for the creation of multifunctional materials. AlFeO_3 (AFO) and $\text{Al}(\text{Fe}_{0.98}\text{Mn}_{0.02})\text{O}_3$ (AMFO), lead-free perovskite materials, have been synthesized by solid-state reaction technique using planetary ball milling process, and their structural, electrical, and magnetic properties were investigated by X-ray diffraction (XRD) technique, Field emission scanning electron microscope (FESEM), Vibrating sample magnetometer and impedance analyzer. XRD analysis shows that synthesized samples have rhombohedral symmetry with space group R-3c. FESEM image shows that grains are segregated into different clusters with a size distribution from 183 to 320 nm. All the samples display a decreasing trend in the real and imaginary part of the dielectric constant with increasing frequency which is due to the reduction of space charge polarization. At higher frequencies, dielectric loss is low due to inhibition of domain wall motion. At room temperature, the initial increase in the real part of permeability (μ') is attributed to the combined effect of magnetic dipolar orientations and spin rotation. At 77 K, sudden falls of μ' originate from the damping mechanism of spins. The imaginary part of permeability decreases exponentially with increasing frequency. In DC magnetization measurements, both AFO and AFMO show antiferromagnetic nature at room temperature.

CONTENTS

Acknowledgments	V
Abstract	VI
Contents	VII
List of Figures	X
List of Tables	XII
List of Symbols and Abbreviations	XIII

1. INTRODUCTION

1.1	Introduction	1
1.2	Motivation	2
1.3	Objectives	3
1.4	Outline of the Thesis	3

2. LITERATURE REVIEW AND THEORETICAL ASPECTS

2.1	Review of Earlier Works	4
2.2	Theoretical Aspects	7
2.2.1	Multiferroics	7
2.2.2	Origin of multiferroicity	8
2.2.3	Applications of multiferroics	8
2.2.4	Multiferroic composites	9
2.2.5	Ferroelectricity	9
2.2.6	Structure of ferroelectric materials	10
2.2.7	Perovskite structure	10
2.2.8	Properties of perovskite materials	11
2.2.8.1	Applications	11
2.2.9	Magnetoelectric effect	12
2.2.10	Magnetodielectric effect	13
2.2.11	Magnetic properties	13
2.2.12	Magnetic materials	15
2.2.13	Mechanism of permeability	16

2.2.14	Electric properties	17
2.2.14.1	Dielectric properties	17
2.2.15	Dependence of dielectric properties on various factors	17
2.2.15.1	Dependence of dielectric properties on frequency	18
2.2.16	Factors affecting dielectric losses	18
2.3	Magnetic and Dielectric Parameters	19
2.3.1	Magnetization	19
2.3.2	Permeability	19
2.3.3	Dielectric parameters	21
2.3.3.1	Dielectric constant	21
2.3.3.2	Dielectric loss	21
2.3.3.3	Electrical impedance	23
2.4	Properties of AlFeO_3	24
2.4.1	Structural, magnetic, dielectric, and related properties of AlFeO_3	24
2.4.2	AlFeO_3 as a multiferroic material	25
2.4.3	AlFeO_3 as a perovskite material	25
2.4.4	Effect of Mn doping	26
3. MATERIALS AND METHODS		
3.1	Solid-State Reaction Technique	28
3.1.1	Ball milling process	28
3.1.2	Synthesis of samples for the present research	29
3.2	Structural Properties Measurements	31
3.2.1	X-ray diffraction technique	31
3.2.2	Field emission scanning electron microscopy	32
3.3	AC Electrical and Magnetic Properties Measurements	32
3.4	DC Magnetic Properties Measurements	32
3.4.1	Vibrating sample magnetometer	32
3.4.1.1	Calibration of vibrating sample magnetometer	33

4. RESULTS AND DISCUSSION

4.1	Structural Properties	34
4.1.1	X-ray diffraction analysis	34
4.1.2	Morphological analysis	36
4.2	AC Electrical Properties	38
4.2.1	The real part of dielectric constant	38
4.2.2	The imaginary part of the dielectric constant	40
4.2.3	Dielectric loss	41
4.2.4	Impedance	42
4.3	AC Magnetic Properties	44
4.3.1	The real part of permeability	44
4.3.2	The imaginary part of permeability	46
4.3.3	Magnetic loss	49
4.3.4	Magnetic modulus	50
4.3.4.1	The Real part of the magnetic modulus	50
4.3.4.2	The imaginary part of the magnetic modulus	52
4.3.4.3	Nyquist plot of magnetic modulus	54
4.4	DC Magnetic Properties	55

5. CONCLUSIONS

5.1	Summary	57
5.2	Suggestions for future work	59
	References	60
	Appendix	70

List of Figures

Fig. 2.1	Relationship between magnetically polarizable and electrically polarizable materials to multiferroics and magnetoelectrics.	7
Fig. 2.2	Relationship between magneto dielectrics and multiferroics.	13
Fig. 2.3	Schematic illustrations of spin interactions for (a) paramagnetic, (b) ferromagnetic ordering, (c) antiferromagnetic ordering, (d) canted antiferromagnet (or weak ferromagnet), and (e) ferrimagnetic ordering.	14
Fig. 2.4	a) Hysteresis loop and b) magnetization as a function of temperature for a typical ferromagnetic material.	15
Fig. 2.5	a) Arrangements of magnetic moments and b) variation of susceptibility and inverse susceptibility with temperature for an antiferromagnetic material.	16
Fig. 2.6	Equivalent circuit diagrams: a) capacitive cell, b) charging and loss current, and c) loss tangent.	22
Fig. 2.7	Magnetic properties oriented in [111] direction.	24
Fig. 2.8	R-3c rhombohedral perovskite unit cell.	26
Fig. 3.1	Ball milling machine.	29
Fig. 3.2	(a) Disk and toroid shaped samples and (b) uniaxial press machine	30
Fig. 3.3	Vibrating sample magnetometer (a) schematic and (b) experimental set-up	33
Fig. 4.1	X-ray diffraction patterns of AFO, AFMO compositions ball-milled for 3 hours and 8 hours.	35
Fig. 4.2	The microstructure of AFO, AFMO compositions ball-milled for 3 hours and 8 hours.	37
Fig. 4.3	The frequency-dependent real part of the dielectric constant of AFO, AFMO compositions ball-milled for 3 hours and 8 hours.	39
Fig. 4.4	The frequency-dependent imaginary part of the dielectric constant of AFO, AFMO compositions ball-milled for 3 hours and 8 hours.	41
Fig. 4.5	The frequency-dependent dielectric loss of AFO, AFMO compositions ball-milled for 3 hours and 8 hours.	42
Fig. 4.6	Impedance as a function of frequency for AFO, AFMO compositions ball-milled for 3 hours and 8 hours.	43

Fig. 4.7	The real part of relative permeability as a function of the frequency of AFO, AFMO compositions ball-milled for 3 hours and 8 hours and measured at room temperature.	45
Fig. 4.8	The real part of relative permeability as a function of the frequency of AFO, AFMO compositions ball-milled for 3 hours and 8 hours and measured at temperature 77 K.	46
Fig. 4.9	The imaginary part of relative permeability as a function of the frequency of AFO, AFMO compositions ball-milled for 3 hours and 8 hours.	48
Fig. 4.10	Frequency-dependent magnetic loss of AFO, AFMO compositions ball-milled for 3 hours and 8 hours and measured at room temperature.	49
Fig. 4.11	Frequency-dependent magnetic loss of AFO, AFMO ball-milled for 3 hours and 8 hours respectively at temperature 77 K.	50
Fig. 4.12	Variation of the real part of magnetic modulus with the frequency of AFO, AFMO compositions ball-milled for 3 hours and 8 hours and measured at room temperature.	51
Fig. 4.13	Variation of the imaginary part of magnetic modulus with the frequency of AFO, AFMO compositions ball-milled for 3 hours and 8 hours and measured at room temperature.	53
Fig. 4.14	Nyquist plot for (a) AFO, AFMO compositions ball-milled for 3 hours and (b) AFO, AFMO compositions ball-milled for 8 hours and measured at room temperature.	54
Fig. 4.15	Effect of Mn doping on M-H loop of AFO, AFMO compositions ball-milled for 3 hours respectively.	56
Fig. 4.16	Effect of Mn doping on M-H loop of AFO, AFMO compositions ball-milled for 8 hours respectively.	56

List of Tables

4.1	The crystal structure, cell parameters, volume and crystallite size of $\text{Al}(\text{Fe}_{1-x}\text{Mn}_x)\text{O}_3$ ($x = 0.00$ and 0.02) compounds ball milled for 3 hours and 8 hours.	35
4.2	Grain size of the compositions $\text{Al}(\text{Fe}_{1-x}\text{Mn}_x)\text{O}_3$ ($x = 0.00$ and 0.02) ball milled for 3 hours and 8 hours.	36
4.3	Characteristic frequency and characteristic relaxation time constant for the samples AFO-3hrs., AFO-8hrs., AFMO-3hrs. and AFMO-8 hrs.	53

List of Symbols and Abbreviations

AFO	Aluminum Iron Oxide
AFMO	Manganese Doped Aluminum Iron Oxide
ME	Magnetoelectric
AFM	Antiferromagnetic
XRD	X-ray Diffraction
λ	X-ray Wavelength
FESEM	Field Emission Scanning Electron Microscopy
VSM	Vibrating Sample Magnetometer
ϵ	Dielectric Constant
ϵ_0	Permittivity in Free Space
Tanδ	Dielectric Loss
Z	Impedance
μ'	Real Part of Permeability
μ''	Imaginary Part of Permeability
M_m'	Real Part of Magnetic Modulus
M_m''	Imaginary Part of Magnetic Modulus
NPS	Nanoparticles
C	Capacitance with Material
C₀	Capacitance in Free Space
Ω	Angular Frequency
H	Magnetic Field
M	Magnetization
Z	Impedance
K	Kelvin

1. INTRODUCTION

1.1 Introduction

Recently, the perovskite-type oxide materials exhibiting Ferro or antiferromagnetic and ferroelectric orderings known as multiferroics, have gained significant scientific and technological attention [1, 2, 3]. ABO_3 type perovskites are of abiding interest to both experimentalists and theoreticians due to their practical applications in catalysis, sensing, magnetoresistance devices, and spintronics [4-7]. It is well-known that $AlFeO_3$ (AFO) is a perovskite-type oxide material and displays piezoelectric, magnetoelectric (ME), and ferromagnetic properties at low temperatures [8, 9]. For environmental and public health safety reasons, the researchers and manufacturers of devices are increasingly interested in reducing or even in extreme cases, eliminating the heavy metals from these materials i.e., in producing lead-free materials. The magnetic ordering in AFO is due to the metal-oxygen-metal antiferromagnetic super-exchange interactions [10, 11]. Therefore, the AFO material has attracted extensive attention because of its potential applications in ME sensors and transistors on account of its special magnetic ordering [12, 13]. Another attractive feature is its environment-friendly nature as compared to other lead-based perovskite-type oxide materials [14]. In designing functional devices, a clear knowledge of the structural, electrical, and magnetic properties is essential. AFO is a lead-free ABO_3 type perovskite material. In AFO, the Al and Fe atoms, respectively occupy the A and B positions of the standard ABO_3 perovskite. Thus, the Fe atom is having six-fold coordination inside the oxygen octahedra of perovskite [15]. AFO is expected to exhibit some properties similar to Al_2O_3 or Fe_2O_3 , as it is derived from Fe_2O_3 by the substitution of one Fe^{3+} by Al^{3+} to form a rhombohedral structure [11]. AFO was found to exhibit ferroelectric relaxor and magnetic spin-glass behavior with a weak ferromagnetic ordering [16]. ABO_3 type perovskite oxides with B-site doping have been extensively studied to optimize relevant physical properties such as ferroelectricity, superconductivity, and ferromagnetism in the product phases [17-21]. B cations are known to be substantial determinants of the physical properties of the ABO_3 system. One of the recent developments in this family of perovskite oxides is the discovery of ferroelectricity and magnetic ordering in $AlFeO_3$ material [22, 23]. It is noted that a small amount of Mn doping can not only

increase the resistivity, dielectric and piezoelectric properties but also significantly improve its magnetic properties.

The search for multi-functionalities in a single-phase material is a subject that has been lead to many fundamental and applied studies. Due to the various unexploited aspects in structural, electrical, and magnetic properties in Mn-doped AlFeO_3 compositions, this work aims to discuss the structural, electrical, and magnetic properties in these compositions.

1.2 Motivation

Multiferroics and ME materials are gaining modern technological importance in recent years [1, 2]. This is because they have potential applications in areas where (anti)ferroelectric and (anti)ferromagnetic materials are extensively employed [3, 4]. Natural single-phase multiferroic are rare, and their ME responses are either relatively weak or occur at a temperature too low for practical applications. Though conventional knowledge about ferroelectricity and ferromagnetism reveals their mutually exclusive nature, as this century unfolds, there have been numerous reports in which ferroelectricity arises due to unconventional reasons [5]. This has indeed opened up doors for research in this area, both experimental and theoretical. Many of the materials neglected in the past, demand reinvestigation. Multiferroic and the ME effect provide a rich area for exploring fundamental science. In this work, It is basically looked into the $\text{Al}(\text{Fe}_{1-x}\text{Mn}_x)\text{O}_3$ ($x = 0.00$ and 0.02) compositions. There are a few experimental reports on the preparation and physicochemical properties of the rhombohedral AlFeO_3 based compositions. This is the motivation for this study on the structural, electrical, and magnetic properties of rhombohedral structured AFO. The lead-free AFO-based compounds are attractive multiferroic materials, as those present piezoelectricity and ferrimagnetism at low temperatures [6]. There have been previous reports about these compositions but these are scattered and are not consolidated. So, a detailed study of the structural, dielectric, and magnetic properties of these compositions is conducted. In this project, a high-energy planetary ball milling technique is used to prepare $\text{Al}(\text{Fe}_{1-x}\text{Mn}_x)\text{O}_3$ ($x = 0.00, 0.02$) compounds by crushing, grinding, and milling the appropriate amount of raw oxide materials Al_2O_3 , Fe_2O_3 , and MnO_2 together. Ball milling boasts several advantages over other systems: the cost of installation and

grinding medium is low, it is suitable for both batch and continuous operation, and applicable for materials of all degrees of hardness.

1.3 Objectives

The main objectives of this research are as follows:

- Synthesis of $\text{Al}(\text{Fe}_{1-x}\text{Mn}_x)\text{O}_3$ ($x = 0.00$ and 0.02) compositions using the planetary ball milling technique at different time durations.
- Study of crystal structure (by X-ray diffraction) and hence determination of lattice parameters of various samples.
- Investigation of surface morphology and microstructural analysis using Field Emission Scanning Electron Microscopy (FESEM).
- Measurement of magnetization as a function of the magnetic field at room temperature by using Vibrating Sample Magnetometer (VSM).
- Investigation of frequency-dependent dielectric properties.
- Measurement of complex initial permeability as a function of frequency at different temperatures.
- Investigation of the effect of Mn doping on structural, electrical, and magnetic properties of the samples.

1.4 Outline of the Thesis

The summary of the thesis is as follows:

In chapter 1, the introduction, motivation, objectives, and outline of the thesis are given.

In chapter 2, literature review, theoretical backgrounds are presented and different parameters which are analyzed are described in detail.

In chapter 3, the methodology in sample preparation and the characterization techniques that are used for different investigations are presented.

In chapter 4, the result and discussion of the research work are presented in detail.

In chapter 5, conclusions and suggestions for future work are presented.

2. LITERATURE REVIEW AND THEORETICAL ASPECTS

2.1 Review of Earlier Works

In the first half of the twentieth century, several major studies have been done by different researchers in different parts of the world for the development of magnetic materials began in Japan by researchers Kato et al. in the 1930 and by J. Snoek of the Philips Research Laboratories in the period 1935-45 in the Netherlands. In 1948, the Neel theory of ferromagnetic provided the theoretical understanding of this type of magnetic material [24]. Nowadays the research interest for the magnetoelectric compounds has been rekindled [1, 25-28], mainly due to the report of Kimura et al., [29] on the existence of the magnetoelectric effect in the frustrated-spin TbMnO_3 compound.

Literature reviews on AFO compositions and the doping effect in AFO materials have been studied extensively to give a broad idea about the structural, magnetic, and electrical properties of AFO based compounds.

Much work has been done to enhance the multiferroic properties of AFO.

Schieber et al. [9] studied the $\text{Al}_{2-x}\text{Fe}_x\text{O}_3$ family of oxides and concluded that the orthorhombic phase is stable in the range ($x = 0.6 - 1.0$). He also reported these oxides to be piezoelectric and magnetized in them to be composed of two non-equivalent sites having opposite magnetic moments.

Saha et al. [10] have investigated AFO, GaFeO_3 as well as oxides of the composition $\text{Al}_{1-x-y}\text{Ga}_x\text{Fe}_{1+y}\text{O}_3$ ($x=0.2$, $y=0.2$) for possible ferroelectricity by carrying out pyroelectric measurements.

Santos et al. [16] investigated the synthesis and ferroic properties of AFO based ceramics. They milled stoichiometric proportions of the precursor's $\alpha\text{-Fe}_2\text{O}_3$ and $\alpha\text{-Al}_2\text{O}_3$ and sintered to obtain AFO ceramics.

Tyagi et al. [30] have deposited thin films of a lead-free magnetoelectric compound AFO using a pulsed laser deposition technique. They observed that the polycrystalline AFO film showed a strong magnetoelastic coupling.

Shirolkar et al. [31] reported the preparation of a rhombohedral phase (space group R3c) AFO nanoparticles (NPS) and their magnetic and ferroelectric properties. They prepared AFO NPS by sol-gel route followed by annealing at 700 °C. They observed that the NPS showed antiferromagnetic nature at room temperature and weak ferroelectric properties near room temperature.

Qiang Li et al. [32] synthesized perovskite-type AFO powders by a modified polyacrylamide gel route using different chelating agents at different pHs. From their X-ray diffraction and Raman results, they observed that the AFO powders synthesized with oxalic acid were rhombohedral structured, while the AFO powders fabricated by using the other chelating agents exhibited orthorhombic structure. They also observed from the scanning electron microscopic images that the particle size of samples with rhombohedral structure is larger than that of the samples with orthorhombic structure.

Wang et al. [33] prepared AFO powders by a modified polyacrylamide gel method and studied their thermal expansion and photoluminescence properties. Their X-ray diffraction analysis indicated that the as-synthesized AFO has the same structure as α -Fe₂O₃ without the presence of any other impurities.

Rao et al. [34] have deposited x -AFO ($0.5 \leq x \leq 1$) epitaxial thin films with low leakage, on SrTiO₃ <111> substrates by Pulsed Laser Deposition technique. They confirmed room temperature ferrimagnetism of the films from the magnetic measurements. Their First principle calculations suggested that ferroelectric domain switching occurs through the shearing of in-plane oxygen layers, and predicted a high polarization value of 24 $\mu\text{C}/\text{cm}^2$.

Hamasaki et al. [35] tried to grow epitaxial AFO films on SrTiO₃ (111) substrates by the pulsed laser deposition technique. Their Piezoresponse force microscopy measurements clearly showed that GaFeO₃-type AFO films have ferroelectricity at room temperature. They also observed AFO film showing pinched-like hysteresis loop with $T_N \sim 317$ K.

Kumar et al. [36] determined the nature of coupled phonons and magnetic excitations in AFO using inelastic light scattering from 5 to 315 K covering a spectral range from 100 to 2200 cm^{-1} and complementary first-principles density functional theory-based calculations.

Shirolkar and Wang et al., [37] synthesized high purity AFO nanoparticles by chemical route to investigate electrical and magnetic properties.

Mohamed and Fuess et al. [38] have doped Mn^{3+} in the Fe^{3+} site and found that transition temperature, saturation magnetization, and coercivity decreased. They have attributed this to the antiferromagnetic coupling between Mn^{3+} and Fe^{3+} ions.

Nagai et al. [39] have reported the corundum (R-3c) phase being stabilized at high pressures.

An important report comes from the experimental work of Bouree et al., [40], wherein they reported the synthesis and detailed study of the crystal structure of AFO. They also studied the magnetic structure of piezoelectric, ferromagnetic, and magnetoelectric properties of AFO from neutron powder diffraction and had found that this compound has four different cation sites which have octahedral and tetrahedral packing of oxygen atoms. They have found tetrahedral packing responsible for the piezoelectricity in this oxide. Fe^{3+} moment calculated by them turned out to be $3.4 \pm 0.3 \mu_{\text{B}}$ which was lower than expected. They had attributed this to the disordered occupancy of cations in the system.

Yuan et al. [41] analyzed the AFO and TiO_2 nanocomposite photocatalysts through X-ray diffraction patterns and predicted that the optical band gap of AFO to be ~ 2.1 eV.

Remeika et al. [21] reported that AFO is isomorphous with GaFeO_3 .

Han et al. [42] showed that GaFeO_3 is isostructural to AFO and nanoparticles with different grain sizes affect the site disorder and as a consequence, the magnetic properties are influenced.

Brown et al. [43] measured the lattice constants and recorded the Mossbauer spectra for $\alpha\text{-Al}_2\text{O}_3$ samples containing Fe^{3+} ions.

2.2 Theoretical Aspects

2.2.1 Multiferroics

Multiferroics were defined as materials that simultaneously possess two or more of the so-called ‘Ferroic’ order parameters such as ferroelectricity, ferromagnetism, ferroelasticity, etc. [44]. Nowadays, multiferroics often refer to a combination of ferroelectricity and magnetism (ferromagnetism, anti-ferromagnetism) in one particular material. So, to place multiferroic materials in their appropriate historical context, one also needs to consider ME materials, in which an electric field modifies the magnetic properties and vice versa. Ferroelectricity also requires that the material should be crystallized in a non-centrosymmetric space group [2]. In multiferroics, the ferroelectric displacement is driven by the A-site cation, and the magnetism arises from a partially filled d shell on the B site [1].

Sometimes the definition of multiferroics is expanded by including non-primary order parameters, such as anti-ferromagnetism or ferrimagnetism i.e.; most of the multiferroic oxides reported are antiferromagnetic, with some of them exhibiting canted anti-ferromagnetism or ferrimagnetism [2].

Multiferroic materials are attractive not only because they have properties of both magnetic and ferroelectric compounds, but also the ME coupling gives an extra degree of freedom in device functionality.

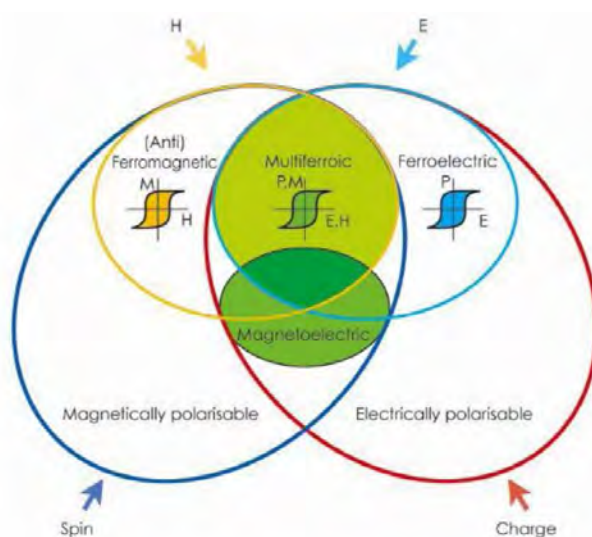


Fig. 2.1 Relationship between magnetically polarizable and electrically polarizable materials to multiferroics and magneto-electrics.

2.2.2 Origin of multiferroicity

In general, the ME effect describes the coupling between electric and magnetic fields in matter. The origin of magnetism is the same in all insulating magnetic materials, the existence of localized electrons in partially filled d or f shells of a transition metal or rare-earth ions, which have a corresponding magnetic moment. However, the absence of d electrons is an advantage for ferroelectricity [45]. Most ferroelectrics are transition metal oxides where the noncentro symmetry arises from the shifting of cations and anions inside the crystal as the positive transition metal ions like to form ‘molecules’ with the negative oxygen ions. These movements are stabilized by the formation of covalent bonds from the hopping of electrons from filled oxygen shells to empty transition metal d shells. One suggestion is the possibility that transition metal ions with occupied d shells are too large to be displaced from the center of oxygen octahedral as commonly found in ferroelectric perovskite however there is not a systematic correlation when the size of the ions is investigated so this is probably not the deciding factor [46].

2.2.3 Applications of multiferroics

Besides a scientific interest in their physical properties, multiferroics have the potential for applications as actuators, switches, magnetic field sensors, or new types of electronic memory devices [47]. The main technological driver for the exploration of multiferroics is their potential for controlling magnetism using electric fields via their ME coupling. Such a capability could be technologically transformative since the production of electric fields is far less energy-intensive than the production of magnetic fields that are used in most existing magnetism-based technologies.

Multiferroic composite structures in bulk form are explored for high sensitivity ac magnetic field sensors and electrically tunable microwave devices such as filters, oscillators, and phase shifters in which the ferri-, ferro-, or antiferromagnetic resonance is tuned electrically instead of magnetically.

Multiferroics have been used to address fundamental questions in cosmology and particle physics [48]. In the first, the fact that an individual electron is an ideal

multiferroic, with any electric dipole moment required by symmetry to adopt the same axis as its magnetic dipole moment, has been exploited to search for the electric dipole moment of the electron.

2.2.4 Multiferroic composites

It remains a challenge to develop good single-phase multiferroics with large magnetization and polarization and strong coupling between them at room temperature. Therefore composites combined with magnetic and ferroelectric materials, either in layers or mixtures, with coupling provided by the interfaces between them, are an attractive and established route to achieving multiferroicity. Several multiferroic oxides have, however, been discovered in the past few years by novel operating mechanisms, the most effective one being ferroelectricity driven by magnetism itself. The multiferroic materials showing simultaneously magnetic and electric ordering in a single phase are relatively rare and their ME response is either relatively weak or occurs at a temperature too low for practical applications. The discovery of several monophasic multiferroic and ME oxides in the past few years, exhibiting magnetically driven ferroelectricity, is quite impressive. In some of the perovskite, the magnetic transition temperature and hence the ferroelectric transition temperature can be varied by tuning the constituent rare earth or transition metal ions, it may be possible to generate multiferroics operating over a wide range of temperatures.

While most of the [45, 49-52] research on multiferroic and ME materials has focused on BiFeO_3 and its limitations necessitate the need to examine other materials such as AlFeO_3 . There are indications in the earlier literature that both GaFeO_3 and AlFeO_3 are piezoelectric [53, 54], and a recent study reports the magnetodielectric effect in these oxides [11]. GaFeO_3 and AlFeO_3 are respectively ferroelectric and multiferroic. They are ferrimagnetic [23, 55], with interesting dielectric properties.

2.2.5 Ferroelectricity

Ferroelectricity is a characteristic of certain materials that have a spontaneous electric polarization that can be reversed by the application of an external electric field [56, 57]. Ferroelectric materials have characteristics of switchable macroscopic polarization. The

formal definition of a ferroelectric material undergoes a phase transition from a high-temperature phase that behaves as an ordinary dielectric to a low-temperature phase that has a spontaneous polarization whose direction can be switched by an applied field. Ferroelectric materials exhibit a wide spectrum of functional properties, including switchable polarization, piezoelectricity, high non-linear optical activity, pyroelectricity, and non-linear dielectric behavior. These properties of ferroelectric materials are crucial for application in electronic devices such as sensors, microactuators, infrared detectors, microwave phase filters, and non-volatile memories.

2.2.6 Structure of ferroelectric materials

The most important structure of ferroelectric ceramics is given below:

- (1) Perovskite type
- (2) Tungsten-Bronze type
- (3) Spinal structure (Layered structure)
- (4) Pyrochloro type

Among these, perovskite ferroelectric ceramic oxides are the most studied because of their wide variety of technological applications.

2.2.7 Perovskite structure

The perovskite structure type is one of the most frequently encountered in solid-state inorganic chemistry. A perovskite has the same type of crystal structure as calcium titanium oxide (CaTiO_3) with oxygen in the edge centers [58]. The general formula for perovskite structure is ABO_3 , where 'A' and 'B' are two cations of very different sizes. The 'A' atoms are larger than the 'B' atoms. The most common perovskite compounds contain oxygen. In the ideal cubic unit cell, 12-coordinated A-site cations sit on the corners of the cube, octahedral O ions on the faces, and the B ion is in the center of the octahedral cage. Due to the flexibility of the corner-sharing octahedra, the perovskite structure can be easily distorted to accommodate a wide range of valence states on both the A- and B- sites by expanding, contracting the lattice, or by rotating the bond angles.

The perovskite crystal structure has corner connected BO_6 octahedra and 12 oxygen coordinated A cations, located in between the eight BO_6 octahedra [59]. However, depending on the ionic radii and electronegativity of the A and B site cations, tilting of the octahedra takes place, which gives rise to lower symmetry structures. As seen from the crystal structure, B site cations are strongly bonded with the oxygen while A site cations have relatively weaker interactions with oxygen. The resulting symmetry of distorted perovskite could be tetragonal, orthorhombic, rhombohedral, or monoclinic [60].

2.2.8 Properties of perovskite materials

From both the theoretical and the application point of view, perovskite materials exhibit many intriguing and interesting properties. The commonly observed features in this family are colossal magnetoresistance, ferroelectricity, superconductivity, charge ordering, spin-dependent transport, high thermopower, and the interplay of structural, magnetic, and transport properties. These compounds are used as sensors and catalyst electrodes in certain types of fuel cells [61] and are candidates for memory devices and spintronics applications [62]. Many superconducting ceramic materials (the high-temperature superconductors) have perovskite-like structures. Perovskites could offer favorable band edge potentials which allow various photoinduced reactions [59].

2.2.8.1 Applications

Perovskites are one of the most important families of materials exhibiting properties suitable for numerous technological applications [63]. The origin of such properties lies in the crystal structure of perovskites. Physical properties of interest to materials science among perovskites include superconductivity, magnetoresistance, ionic conductivity, and a multitude of dielectric properties, which are of great importance in microelectronics and telecommunication. In July 2016, a team of researchers led by Dr. Alexander Weber-Bargioni demonstrated that perovskite photovoltaic cells could reach a theoretical peak efficiency of 31% [64]. Perovskites can be good candidates for use in light-emitting diodes (LEDs) due to their high photoluminescence quantum efficiencies [65].

2.2.9 Magnetoelectric effect

The ME effect denotes any coupling between the magnetic and the electric properties of a material [66, 67]. The first example of such an effect was described by Wilhelm Röntgen in 1888, who found that a dielectric material moving through an electric field would become magnetized [68]. A material where such a coupling is intrinsically present is called a magnetoelectric. The ME effect was experimentally realized in Cr_2O_3 in the 1960s [69-73]. Some promising applications of the ME effect are sensitive detection of magnetic fields, advanced logic devices, and tunable microwave filters [74]. ME effect in a single-phase compound can be described by Landau theory by expressing free energy of the system in terms of the magnetic field, electric field, and their cross-coupling terms as [52]:

$$-F(\mathbf{E}, \mathbf{H}) = \frac{1}{2} \epsilon_0 \epsilon_{ij} E_i E_j + \frac{1}{2} \mu_0 \mu_{ij} H_i H_j + \alpha_{ij} E_i H_j + \frac{\beta_{ijk}}{2} E_i H_j H_k + \frac{\gamma_{ijk}}{2} H_i E_j E_k + \dots \quad (2.1)$$

Here the first term describes the electric response of a material to the applied electric field where ϵ_0 is the permittivity of free space and ϵ_{ij} is the relative permittivity. The second term describes magnetic response with μ_0 as the permeability of free space and μ_{ij} as the relative permeability. The third term is for linear ME coupling and other terms are for higher-order couplings involved. To establish the ME effect, if we differentiate F concerning E_i and set H_i to zero, then we get P_i as a function of H_j as:

$$P_i = \alpha_{ij} H_j + \frac{\beta_{ijk}}{2} H_j H_k + \dots \quad (2.2)$$

Similarly, differentiating F concerning H_i and setting H_i to zero gives M_i as a function of E_j as:

$$\mu_0 M_i = \alpha_{ji} E_j + \frac{\beta_{ijk}}{2} E_j E_k + \dots \quad (2.3)$$

In many materials, linear ME coupling will be small due to smaller values of either ϵ_{ij} or μ_{ij} or both. But this doesn't prevent the existence of higher-order coupling terms like β_{ij} or γ_{ij} . This so-called non-linear coupling is found mainly in materials with reduced dimensionality.

2.2.10 Magnetodielectric effect

ME effects in materials are restricted by symmetry and hence in recent years, a more general term called magnetodielectric effect has been introduced. It was first suggested by Lawas et.al [75]. This describes a more generalized coupling and hence there are no symmetry constraints. Such materials show anomalies in dielectric constant/capacitance when an external magnetic field is applied.

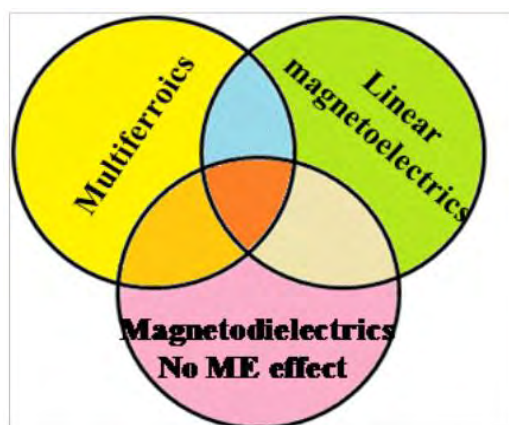


Fig. 2.2 Relationship between magnetodielectric and multiferroics.

Research in multiferroics has reached a very interesting forefront wherein even centrosymmetric materials show interesting signatures of ferroelectricity due to local non-Centro-symmetry [76]. There has been coupling between electric and magnetic order parameters triggered externally by strain etc. [77]. There is also tremendous work done in the field of composites, in which one component is responsible for magnetism and the other for ferroelectricity. ME multiferroics with considerable coupling between electric and magnetic order parameters are also being realized in multiferroics in which ferroelectricity is magnetically induced [29, 78].

2.2.11 Magnetic properties

The magnetic moment of a system measures the strength and the direction of its magnetism. Anything magnetic, like a bar magnet or a loop of electric current, has a magnetic moment. A magnetic moment is a vector quantity, with a magnitude and a

direction. An electron has an electron magnetic dipole moment, generated by the electron's intrinsic spin property, making it an electric charge in motion. There are many different magnetic behavior including para-magnetism, diamagnetism, ferrimagnetism, anti-ferromagnetism and ferromagnetism. An interesting characteristic of transition metals is their ability to form magnets. Metal complexes that have unpaired electrons are magnetic. Since the last electrons reside in the d orbitals, this magnetism must be due to having unpaired d electrons. The spin of a single electron is denoted by the quantum number m_s and is negated when the electron is paired with another but creates a weak magnetic field when the electron is unpaired.

All materials in nature possess a general form of diamagnetic response to an applied magnetic field [79]. There are several other magnetic phenomena present in some inorganic solids caused by unpaired electrons usually located on metal cations. The different effects for a schematic are shown in Fig. 2.4 [80].

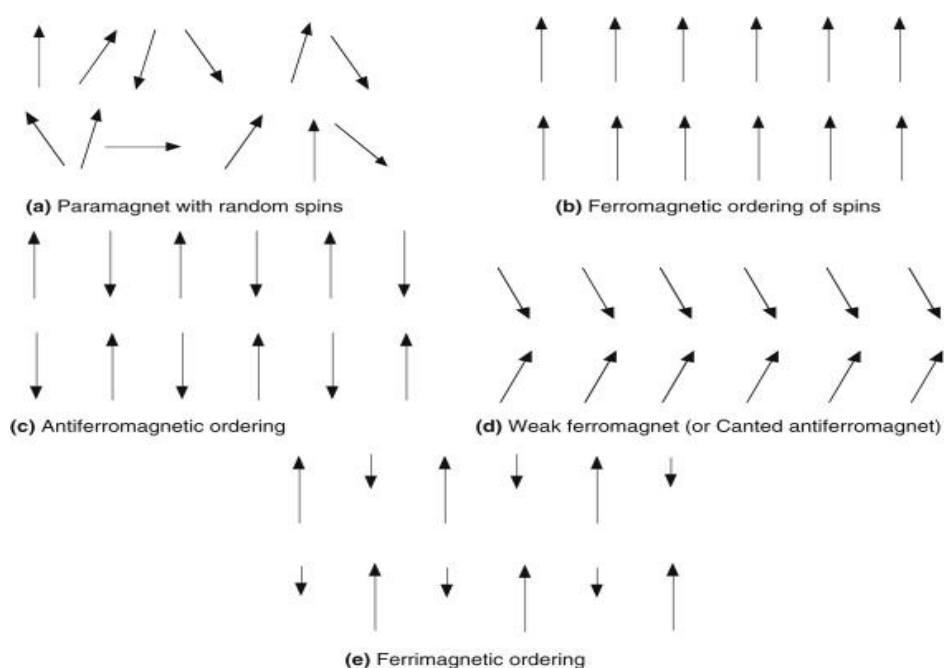


Fig. 2.3 Schematic illustrations of (a) paramagnetic, (b) ferromagnetic, (c) antiferromagnetic, (d) canted antiferromagnet, and (e) ferrimagnetic ordering, respectively.

2.2.12 Magnetic materials

The first magnetic material known to mankind was loadstone (magnetite, Fe_3O_4) [81]. Magnetic materials are classified differently based on their response to the magnetic field. If these materials repel the external field then they are termed diamagnetic materials [82]. Materials whose moments are randomly oriented but tend to align in the direction of the field when an external magnetic field is applied are called paramagnetic materials.

There is yet another class of compounds in which moments are coupled to each other through exchange forces. These materials exhibit magnetic domain structures. The magnetization will be uniform within each domain. Several of these domains arrange randomly giving a net zero magnetization in the absence of an external magnetic field. But when the magnetic field is applied they tend to magnetize spontaneously reaching a maximum value called saturation magnetization (M_s). Even after the removal of the field, these materials tend to retain the memory of the applied field, which is called the remanent magnetization (M_R). These materials hence display a hysteretic behavior in an applied field. At very high temperatures exchange forces are overcome by thermal fluctuations and hence these materials behave paramagnetically above T_c . These materials known as ferromagnetic materials are characterized by a positive Weiss constant.

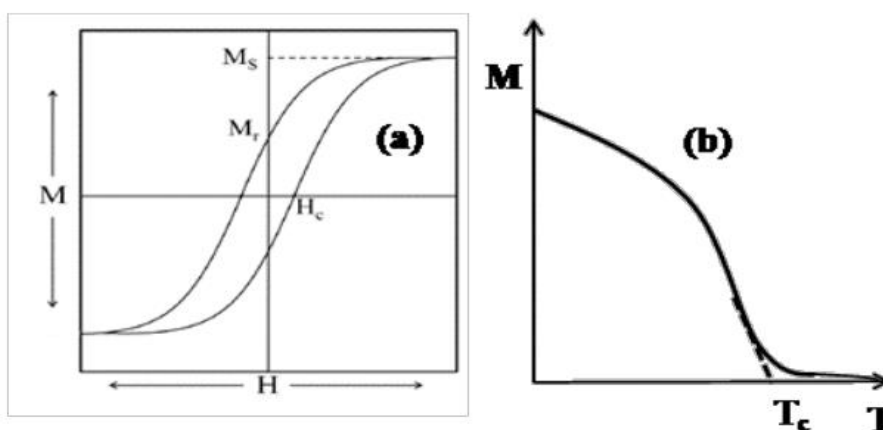


Fig. 2.4 (a) Hysteresis loop and (b) variation of magnetization as a function of temperature for a typical ferromagnetic material.

There are some materials in which neighboring domains are arranged antiparallel to each other giving rise to a net-zero magnetic moment. These are called anti-ferromagnetic materials (Fig. 2.7). These materials are magnetically ordered below T_N and behave paramagnetically above this temperature with a negative Weiss constant.

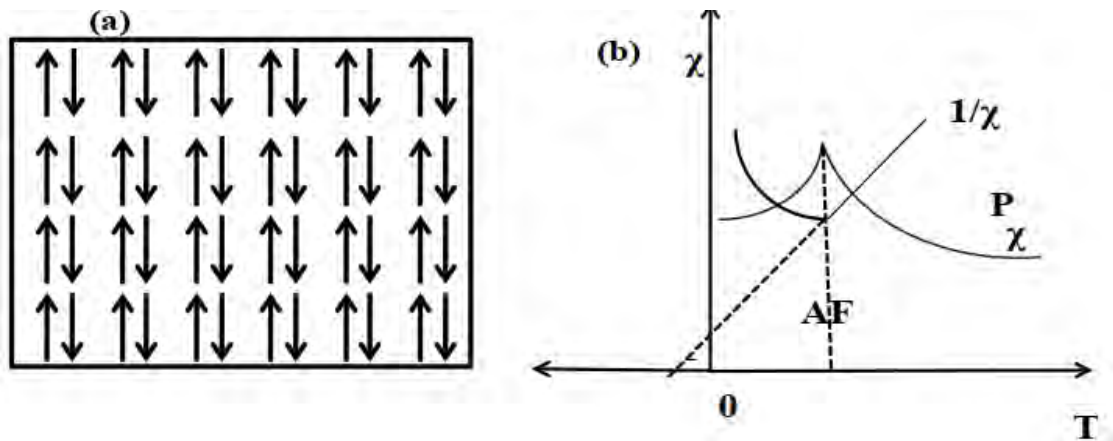


Fig. 2.5 (a) Arrangements of magnetic moments and (b) variation of susceptibility and inverse susceptibility with temperature for an antiferromagnetic material.

If the moments in the oppositely aligned sublattices are unequal then a weak ferromagnetic-like behavior remains. These materials are called ferrimagnetic materials.

2.2.13 Mechanism of permeability

The mechanisms of permeability can be explained as follows: A demagnetized magnetic material is divided into several Weiss domains separated by Bloch walls. In each domain, all the magnetic moments are oriented in parallel and the magnetization has its saturation value M_s . In the walls the magnetization direction changes gradually from the direction of magnetization in one domain to that in the next. The equilibrium positions of the walls result from the interactions with the magnetization in neighboring domains and the influence of pores; crystal boundaries and chemical inhomogeneity which tend to favor certain wall positions.

2.2.14 Electrical properties

The investigations into electrical properties are essential for their use in various applications as dielectric behavior measurements; i.e., (dielectric constant, dielectric loss factor, impedance, etc.) as a function of frequency.

2.2.14.1 Dielectric properties

A material is classified as “dielectric” if it can store energy when an external electric field is applied. These properties are not constant; they can change with frequency, temperature, orientation, mixture, pressure, and molecule structure of the material. For most solids, there is no net separation of positive and negative charges; that there is no net dipole moment. The molecules of solids are arranged in such a way that the unit cell of the crystal has no net dipole moment. If such a solid is placed in the electric field then the field is induced in the solid which opposes the applied electric field. This field arises from the two sources, a distortion of the electron cloud of the atoms or molecules and a slight movement of the atoms themselves. The average dipole moment per unit volume induced in the solid is the electrical polarization and is proportional to the applied electric field. The polarizability (α) of the dielectric is defined by [83]:

$$P = \alpha E$$

Where, P is the dipole moment induced by the local electric field, E.

The complex permittivity relative to free space is represented as $\epsilon = \epsilon' - j\epsilon''$, where ϵ' is the dielectric constant and ϵ'' is the dielectric loss factor. The real part of permittivity represents the energy storage capability in the electric field in the dielectric material, and the imaginary part represents the energy dissipation capability of the dielectric by which energy from the electric field is converted into heat energy in the dielectric. Often, the loss angle of dielectrics is of interest, and the tangent of the loss angle δ is used, $\tan \delta = \epsilon''/\epsilon'$.

2.2.15 Dependence of dielectric properties on various factors

The dielectric properties of most materials vary with several influencing factors [84]. The dielectric properties also depend on the frequency of the applied alternating electric

field, the temperature of the material, and composition, and structure of the material. The dielectric properties of materials are dependent on the chemical composition and especially on the presence of mobile ions and the permanent dipole moments associated with molecules making up the material of interest.

The dielectric constant is the property of a dielectric medium that determines the force of the electric charges that exert on the dielectric. The value of ϵ' also depends on several external factors, such as the frequency of the voltage applied to the dielectric, temperature, particle size, etc.

2.2.15.1 Dependence of dielectric properties on frequency

Except for some extremely low-loss materials, the dielectric properties of most materials vary considerably with the frequency of the applied electric fields. This frequency dependence has been discussed previously [84-86]. An important phenomenon contributing to the frequency dependence of the dielectric properties is the polarization, arising from the orientation with the imposed electric field of molecules which have permanent dipole moments. The mathematical formulation developed by Debye to describe the permittivity for pure polar materials [87] can be expressed as,

$$\epsilon = \epsilon_{\infty} + \frac{\epsilon_s - \epsilon_{\infty}}{1 + j\omega\tau}$$

Where, $\omega = 2\pi f$ is the angular frequency, ϵ_{∞} represents the dielectric constant at frequencies so high that molecular orientation does not have time to contribute to the polarization, ϵ_s represents the static dielectric constant, i.e., the value at zero frequency (dc value), and τ is the relaxation time in seconds, the period associated with time for the dipoles to revert to random orientation when the electric field is removed.

2.2.16 Factors affecting dielectric losses

$\tan\delta$ is very sensitive to humidity. Hence the microwave measurements should be done in an air-conditioned room. The samples should be heated in a furnace to remove the moisture before starting the experiments. A low loss material, it should contain the lowest possible concentration of dipoles and charge carriers with the lowest possible

mobility. However, it is a fact that most technically important insulating materials are far from very pure and often contain deliberate or accidental admixtures of substances that are necessary for their processing. The disordered charge distributions in the crystal lattice also contribute to dielectric loss. Dielectric losses occur if the charge distribution in the crystal deviates from perfect periodicity. In 1964, Schlomann reported that in ionic non-conducting crystals, the loss tangent increases when the ions are distributed disorderly in such a way that they break the periodic arrangement of atoms in the crystal [88]. The loss tangent depends strongly on the spatial correlation between charge deviations. He also reported that the loss tangent is negligible if the disordered charge distribution in the crystal maintains the charge neutrality within a short range of the order of lattice constant.

2.3 Magnetic and Dielectric Parameters

2.3.1 Magnetization

Magnetization is the vector field that expresses the density of permanent or induced magnetic dipole moments in a magnetic material. The origin of the magnetic moments responsible for magnetization can be either microscopic electric currents resulting from the motion of electrons in atoms or the spin of the electrons or the nuclei. Net magnetization results from the response of a material to an external magnetic field, together with any unbalanced magnetic dipole moments that may be inherent in the material itself; for example, in ferromagnets. Magnetization is not always homogeneous within a body, but rather varies between different points. Magnetization also describes how a material responds to an applied magnetic field as well as the way the material changes the magnetic field and can be used to calculate the forces that result from those interactions. Physicists and engineers define magnetization as the quantity of magnetic moment per unit volume. It is represented by M .

2.3.2 Permeability

Permeability (μ) is defined as the proportionality constant between the magnetic field induction B and applied field intensity H :

$$B = \mu H \quad (2.4)$$

If the applied field is very low, approaching zero, the ratio is called the initial permeability (μ_i) and is given by,

$$\mu_i = \Delta B / \Delta H \quad (2.5)$$

Where $\Delta H \rightarrow 0$

This simple definition needs further sophistication. A magnetic material subjected to an AC magnetic field can be written as,

$$H = H_0 e^{i\omega t} \quad (2.6)$$

It is observed that the magnetic flux density B lag behind H. This is caused due to the presence of various losses and is thus expressed as,

$$B = B_0 e^{i(\omega t - \delta)} \quad (2.7)$$

Here δ is the phase angle that marks the delay of B with respect to H. μ is then given by,

$$\mu = \frac{B}{H} = B_0 e^{i(\omega t - \delta)} / H_0 e^{i\omega t} = B_0 e^{-i\delta} / H_0 = (B_0 \cos \delta / H_0) - (i B_0 \sin \delta / H_0) = \mu' - i\mu'' \quad (2.8)$$

$$\text{where, } \mu' = B_0 \cos \delta / H_0 \quad (2.9)$$

$$\mu'' = B_0 \sin \delta / H_0 \quad (2.10)$$

The real part (μ') of complex initial permeability (μ) represents the component of B which is in phase with H, so it corresponds to the normal permeability. If there are no losses, it should have $\mu = \mu'$. The imaginary part (μ'') corresponds to that of B, which is delayed by phase angle 90° from H [89, 90]. The presence of such a component requires a supply of energy to maintain the alternating magnetization, regardless of the origin of delay.

The curves that show the variation of both μ' and μ'' with frequency are called the magnetic spectrum or permeability spectrum of the material [89]. The variation of permeability with frequency is referred to as dispersion. The measurement of complex permeability gives us valuable information about the nature of domain walls and their movements. In dynamic measurements, the eddy current loss is very important. This occurs due to the irreversible domain wall movements. The permeability of a ferrimagnetic substance is the combined effect of the wall permeability and rotational permeability mechanisms.

2.3.3 Dielectric parameters

2.3.3.1 Dielectric constant

The dielectric constant (ϵ') was determined using LCR Meter Bridge. For this purpose silver paint was applied on both sides of the pellets to make good contacts with conducting wires. The dielectric constant is given by the relation:

$$\epsilon' = \frac{Cd}{\epsilon_0 A} \quad (2.11)$$

Here, C is the capacitance of the material, ϵ_0 is the permittivity of the free space and has a value of $(8.854 \times 10^{-12} \text{ Fm}^{-1})$, d is the thickness of the pellet in meters and A is the cross-sectional area of the flat surface of the pellet [91].

ϵ' is an intrinsic property of a material and a measure of the ability of the material to store electric charge relative to a vacuum.

Capacitance is the ratio of the change in an electric charge in a system to the corresponding change in its electric potential. The capacitance is a function only of the permittivity of the dielectric material between the plates of the capacitor. It is clear from equation (2.9) that, the higher the ϵ' the higher the capacitance of the capacitor. This is the only variable left with the material scientist to increase the capacitance per unit volume value of capacitor for modern electronics applications.

2.3.3.2 Dielectric loss

Friction is a macroscopic concept and its explanation in terms of models conceived at a microscopic level has presented difficulties in many branches of physics. Dielectric loss is a special type of friction and the classical and quantum statistical mechanical theories of dielectric loss present the familiar difficulties of principle encountered in a theory of dissipation. Every type of dissipation (dielectric loss) is connected with the motions of charge carriers. The effect of their movements in an electric field is called polarization. The total polarization is the sum of various contributions, e.g. electronic polarization due to the relative displacement of electrons and nuclei, dipolar polarization due to orientation of dipoles, and interfacial or Maxwell-Wagner polarization when there are boundaries between the components of a heterogeneous system. The occurrence of dielectric loss can generally be understood as follows: at very low frequencies the

polarization easily follows the alternating field, thus its contribution to the dielectric constant is maximal, and no loss occurs. At very high frequencies the field alternates too fast for polarization to arise and there is no contribution to the dielectric constant, and no energy lost in the medium. Somewhere between these two extremes, the polarization begins to lag behind the field, and energy is dissipated. An ideal dielectric would allow no flow of electronic charge, only a displacement of charge via polarization. If a plate of such ideal material was placed between the capacitive cell and a dc voltage was applied, the current through the circuit would decay exponentially to zero with time. But this would not be the case if an alternating (sine wave) electric field was applied.

For real dielectric material, the current I has two vector components, real I_R and imaginary I_C .

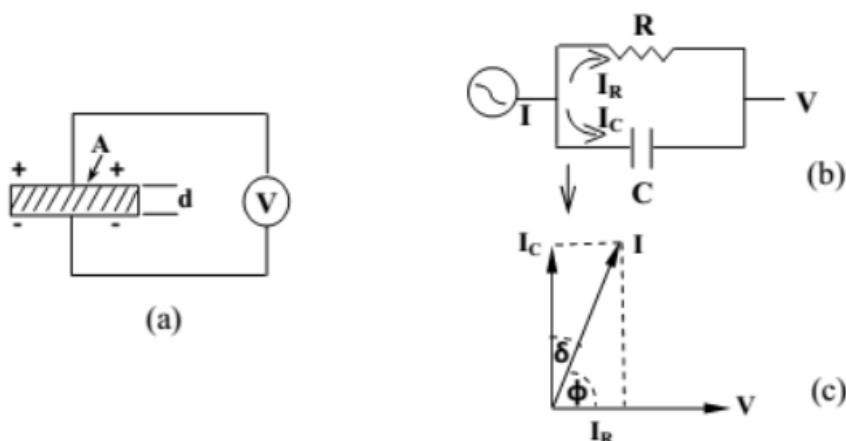


Fig. 2.6 Equivalent circuit diagrams: a) capacitive cell, b) charging and loss current, and c) loss tangent.

The condition of a loss (not so good) dielectric is illustrated in Fig. 2.10 as an equivalent circuit analogous to resistance in parallel with the capacitor. The current I_C represents a (watt less) capacitive current proportional to the charge stored in the capacitor. It is frequency dependent and leads the voltage by 90° . On the other hand, the current I_R is an ac conduction current in phase with the voltage V , which represents the energy loss or power dissipated in the dielectric. The resultant angle between the current and the voltage is ϕ somewhat less than 90° . The current in a real capacitor lags slightly behind what it would be in an ideal capacitor. The angle of lag is defined as δ and the amount of lag becomes $\tan\delta$ or loss tangent.

$$\text{By definition, } \tan\delta = \frac{\epsilon''}{\epsilon'}$$

Dielectric loss is often attributed to ion migration, ion vibration, deformation, and electric polarization. Ion migration is particularly important and strongly affected by temperature and frequency.

2.3.3.3 Electrical impedance

Electrical impedance is the measure of the opposition that a circuit presents to a current when a voltage is applied. The term complex impedance may be used interchangeably. Quantitatively, the impedance of a two-terminal circuit element is the ratio of the complex representation of a sinusoidal voltage between its terminals to the complex representation of the current flowing through it [92]. In general, it depends upon the frequency of the sinusoidal voltage.

Impedance extends the concept of resistance to the AC circuit and possesses both magnitude and phase, unlike resistance, which has only magnitude. When a circuit is driven with direct current (DC), there is no distinction between impedance and resistance; the latter can be thought of as impedance with zero phase angle.

The notion of impedance is useful for performing AC analysis of electrical networks because it allows relating sinusoidal voltages and currents by a simple linear law. In multiple port networks, the two-terminal definition of impedance is inadequate, but the complex voltages at the ports and the currents flowing through them are still linearly related by the impedance matrix [92].

Impedance is a complex number, with the same units as resistance, for which the SI unit is the ohm (Ω). Its symbol is usually Z . However, Cartesian complex number representation is often more powerful for circuit analysis purposes. Instruments used to measure the electrical impedance are called impedance analyzers.

2.4 Properties of AlFeO₃

2.4.1 Structural, magnetic, dielectric, and related properties of AlFeO₃

AFO is an ABO₃ type perovskite material, which retains a collinear ferrimagnetic structure with Néel temperature (T_N) [15, 35]. The magnetic ordering in AFO is due to the metal-oxygen-metal antiferromagnetic superexchange interactions [10, 11]. In AFO, the Al and Fe atoms, respectively occupy the A and B positions of the ABO₃ perovskite. Thus, the Fe atom is having six-fold coordination inside the oxygen octahedra of perovskite. Lacerda et al. [93] reported that the AFO is a weak ferromagnetic material and potential alternatives to develop magnetic or multiferroic devices. They also reported that the magnetism in $R\bar{3}c$ structure was influenced by intrinsic cluster orientation within $R\bar{3}c$ structure, hence α and β electrons are both oriented in the [1 1 1] direction as expected for these structures [94, 95]. Magnetic resultant is oriented along [1 1 1] direction of the unit cell.

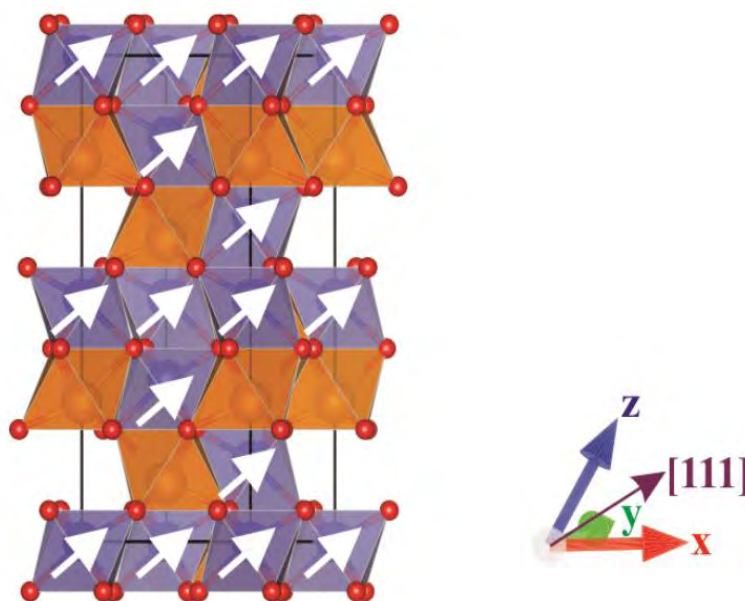


Fig. 2.7 Magnetic properties oriented in [1 1 1] direction [93].

AFO is expected to exhibit some properties similar to Al₂O₃ or Fe₂O₃, as it is derived from Fe₂O₃ by the substitution of one Fe³⁺ by Al³⁺ to form orthorhombic or rhombohedral structure [11]. It has been recently reported that AFO, shows FM

properties [10]. Kumar et al., [36] reported that AFO exhibits ferrimagnetism with a paramagnetic to FM transition temperature $T_c \approx 250$ K [40, 96].

Saha et al. [97] concluded that, from the energies of the ferromagnetically and antiferromagnetically ordered states of AFO, it became clear that the AFM state is more stable than the FM one.

The aluminum iron oxide (AlFeO_3), a room temperature ferroelectric relaxor and magnetic spin-glass compound, emerges as a new single-phase lead-free material that can exhibit magnetoelectricity at room temperature [16, 22, 98]. Relaxors are materials with short-range polarization ordering and exhibit highly frequency-dependent dielectric properties [99].

2.4.2 AlFeO_3 as a multiferroic material

The lead-free AFO-based compounds are attractive multiferroic materials, as those present piezoelectricity and ferrimagnetism at low temperatures [9, 22, 23, 98]. Lead-free AFO and AFO based composite materials offer a lower environmental impact (lead-free) and higher spontaneous magnetization in comparison to other lead-based multiferroics [100]. The attractive feature of AFO is its environment-friendly nature as compared to other lead-based multiferroics [36]. Vibrational properties which bear signatures of structure and magnetic orders are central to the ME behavior of many multiferroics.

2.4.3 AlFeO_3 as a perovskite material

AFO is an ABO_3 type perovskite material where Al and Fe atoms, respectively occupy the A and B positions [101]. The perovskite is a true engineering ceramic material with applications spanning energy production, environmental containment, and communications.

However, in this study both the A and B cations adopt a trivalent state. For the $\text{A}^{3+}\text{B}^{3+}\text{O}_3$ perovskite like AFO, the most symmetric structure is a rhombohedral structure with the space group $R\bar{3}c$, which involves a rotation of the BO_6 octahedra concerning the cubic structure. Thus, the Fe atom is having six-fold coordination inside

the oxygen octahedra of perovskite and Al is in the inter-octahedral space. However, this distortion from the perfect cubic symmetry is slight [1 0 0].

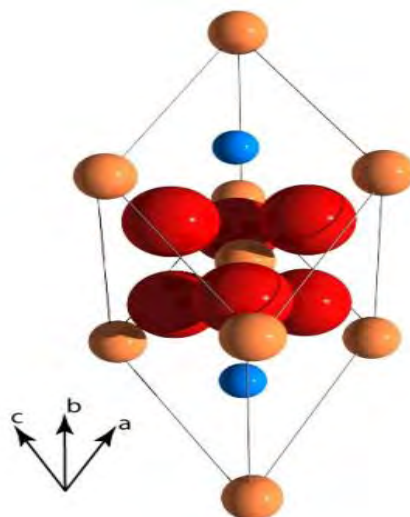


Fig. 2.8 R-3c rhombohedral perovskite unit cell. [102].

However, with decreasing A cation size, a point will be reached where the cations will be too small to remain in contact with the anions in the cubic structure. Therefore the B-O-B links bend slightly, tilting the BO_6 octahedra to bring some anions into contact with the A cations.

AFO is a well-known ABO_3 type perovskite oxide material and exhibits a piezoelectric, ME, and FM effect at low temperatures [8, 9, 40, 98, 103, 104]. AFO exists in two different phases, orthorhombic and rhombohedral [15]. The perovskite-type oxide materials with a low thermal expansion are of great research interest due to their diverse applications from environmental emissions reduction to telecommunications applications [105]. Thus Fe is in six-fold coordination inside the octahedra and Al is in the inter-octahedral space.

2.4.4 Effect of Mn doping

Manganese is a particularly interesting element for substitution because it easily changes its oxidation state, furthermore, the ionic radii of Fe^{3+} and Mn^{2+} are 0.69 Å and 0.67 Å which are practically identical [106]. Even though there are five 3d electrons and

an effective magnetic moment of $\mu_{\text{eff}} = 5.9 \mu_{\text{B}}$ for both Fe^{3+} and Mn^{2+} , the magnetic interaction is affected by the substitution [38]. When Mn is substituted for the Fe site, ferroelectric properties were observed to improve [107].

It is being thought that the advantage of Mn-doped AFO lies in that Mn possesses magnetic activity and the multivalent states of Mn ions enable the crystal to compensate for the charge. Mukherjee et al. reported that Y and Mn co-doping is a valid means to redress various problems relevant to device application [108].

3. MATERIALS AND METHODS

3.1 Solid-State Reaction Technique

To prepare the studied samples, a solid-state reaction technique has been used. The solid-state reaction method is well appreciated for the large-scale production of bulk ceramic powders. It requires low-cost precursors which are readily available and needs an easier preparation technique. This process starts with various solid compounds as raw materials. After stoichiometric calculation, the raw materials are mixed properly and ground by hand using a motor and vessel. The grinding times remain around 5-6 hours. The sample wastage and contamination with organic and inorganic particles present in the atmosphere may occur during the grinding process and cautions should be taken to prevent it. After proper grinding, the sample is fired in a high-temperature furnace between 1000-1500°C for initial phase formation. Then several intermediate steps are needed to get the product sample. These steps are calcination, pelletization, and sintering.

3.1.1 Ball milling process

Mechanical ball milling is one of the most common operations in the processing of solids. The mechanical action of ball milling can release chemical reactions and the simplest effect of ball milling is size reduction. When magnetically ordered materials are milled then the small particle size results in the superparamagnetic relaxation phenomena. The initiation of solid-state reactions by ball milling offers interesting and technologically promising new possibilities. A particularly attractive area is the application of mechanochemical processing for low-temperature, solvent-free synthesis of inorganic materials. Milling is carried out to fulfill twofold purposes, one is to reduce the particle size and another is to mix the raw materials homogeneously. Both finer particles and homogeneity of raw powders ease the diffusion-controlled solid-state reactions.



Fig. 3.1 Ball milling machine

Ball milling boasts several advantages over other systems: the cost of installation and grinding medium is low, it is suitable for both batch and continuous operation, and applicable for materials of all degrees of hardness.

Here in this project, we used a high-energy planetary ball mill to prepare $\text{Al}(\text{Fe}_{1-x}\text{Mn}_x)\text{O}_3$ ($x = 0.00, 0.02$) compounds by crushing, grinding, and milling the appropriate amount of raw oxide materials Al_2O_3 , Fe_2O_3 and MnO_2 together.

3.1.2 Synthesis of samples for the present research

$\text{Al}(\text{Fe}_{1-x}\text{Mn}_x)\text{O}_3$ ceramics with $x = 0.00$ and 0.02 were prepared by standard solid-state reaction method. High purity of Al_2O_3 , Fe_2O_3 , and MnO_2 was used for $\text{Al}(\text{Fe}_{1-x}\text{Mn}_x)\text{O}_3$ ($X=0.00$ and 0.02). Appropriate amounts of reactants were weighed according to their stoichiometric proportions. The raw materials were weighed separately by using an electronic digital analytical balance and then well mixed and ground in an agate mortar for 3 hours using acetone as a mixing medium. Then the ground powders were pre-calcined at 300°C for 30 minutes. After that, the powder samples were further ground by planetary ball mill for 3 hours and 8 hours respectively to make separate samples for comparative studies. Then the ball-milled samples were calcined at 400°C for 4 hours and cooled to room temperature naturally. When room temperature was attained the

powders were re-ground again for 30 minutes by adding a small amount of polyvinyl acetate (PVA) as a binder. Finally, the powders were pressed into pellets and rings using a uniaxial press.

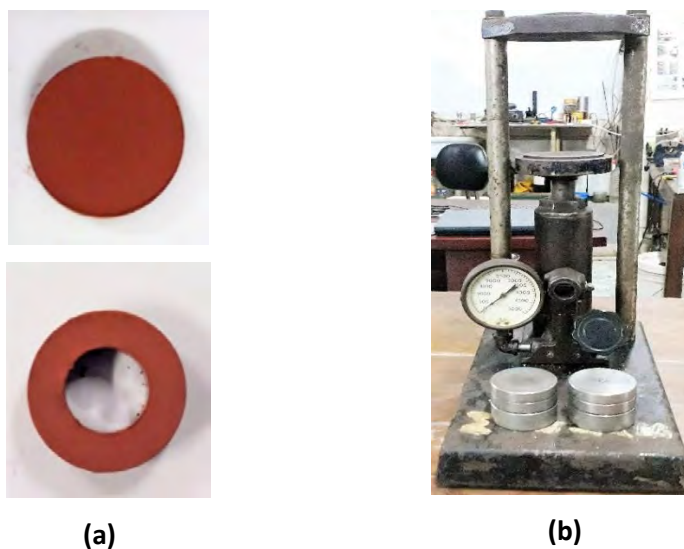
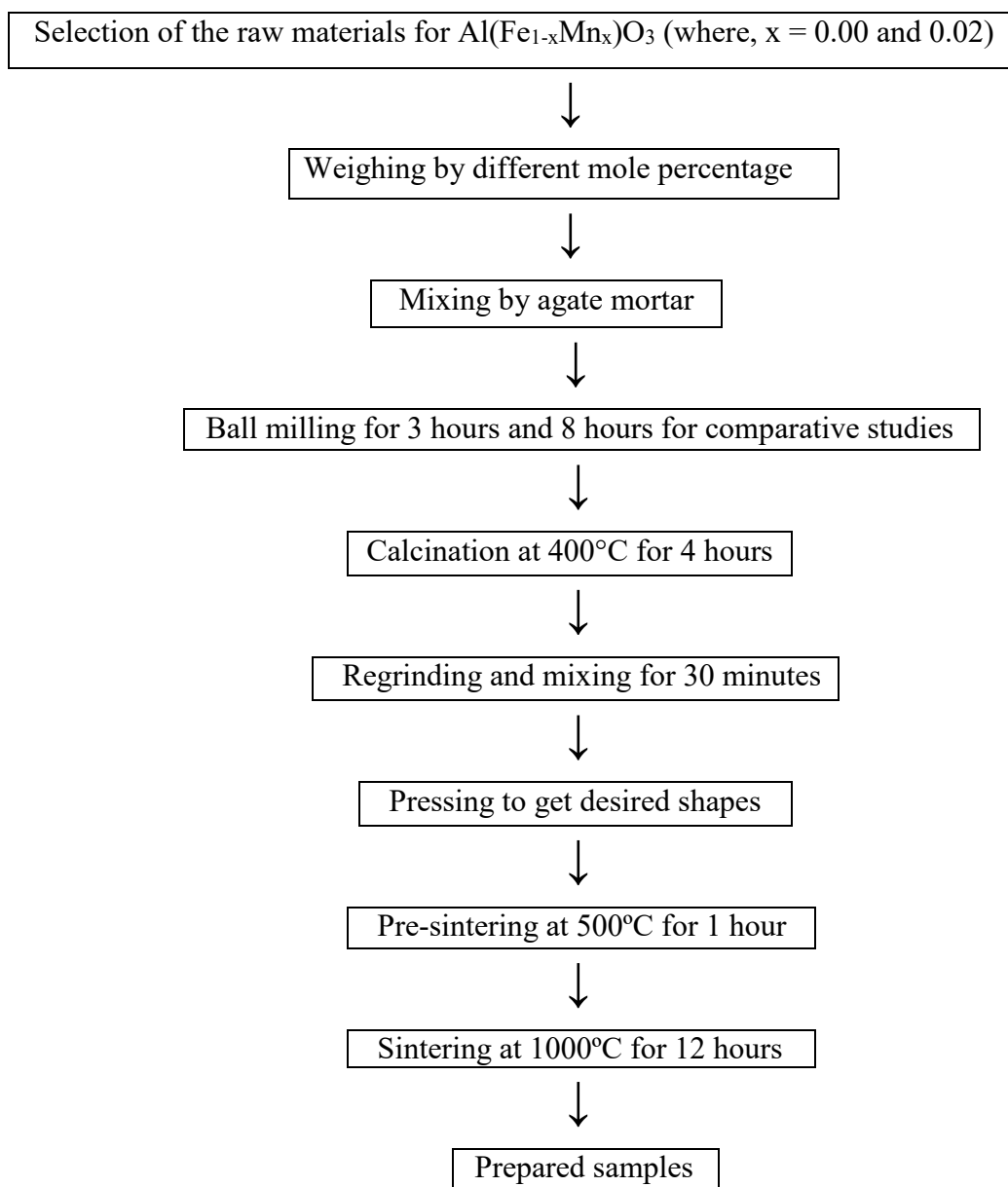


Fig. 3.2 (a) Disks and toroid shaped samples and (b) uniaxial press machine

Pellets and rings were then inserted into the furnace for sintering. Sintering was done at 1000°C for 12 hours to get an equal type of grain size and dipole moment orientation. The cooling process was natural in the air. The pellets and rings were then rubbed using fine sandpaper to have a smooth surface and both were ready for measurements.

The flow chart of the sample preparation process is shown below



3.2 Structural Properties Measurements

3.2.1 X-ray diffraction technique

The XRD technique is commonly used in analytical characterization to gain crystallographic information of crystals. The main function of an XRD instrument is to determine the crystallographic structure, phase structure, atomic and molecular structure of crystalline materials. Since each material possesses its own unique XRD spectra, hence quantitative and qualitative analysis can be carried out from this technique. In the

XRD technique, the crystalline structure of crystalline material causes a beam of incident X-rays to diffract into many specific directions. Powder XRD is extensively used for the identification of phases by measuring the intensities and diffraction angles of these diffracted beams.

3.2.2 Field emission scanning electron microscopy

FESEM is a widely used technique that provides topographical and elemental information at higher magnification with virtually unlimited depth of field. The FESEM is a type of microscopy that gives more clear and magnified images scanning with high-energy electrons.

3.3 AC Electrical and Magnetic Properties Measurements

The study of dielectric properties concerns the storage and dissipation of electric and magnetic energy in materials [109, 110]. Dielectrics are important for explaining various phenomena in electronics, optics, solid-state physics, and cell biophysics. In this experiment, the dielectric properties were measured using a Wayne-Kerr 6500B Impedance Analyzer. The dielectric properties measurements on pellet and toroid-shaped specimens were carried out as a function of frequency in the high-frequency range at room temperature and temperature 77 K, respectively.

To measure dielectric properties, the pellet-shaped samples were polished properly to remove roughness or contamination of any other oxides on the surface during sintering, and samples were painted with conducting silver paste on both sides to ensure good electrical contacts.

3.4 DC Magnetic Properties Measurements

3.4.1 Vibrating sample magnetometer

A VSM is a scientific instrument that measures the magnetic properties of materials. The vibrating component causes a change in the magnetic field of the sample, which generates an electrical field in a coil based on Faraday's law of induction.

If the sample is placed within a uniform magnetic field H , a magnetization M will be induced in the sample. A known standard sample (generally Ni) is usually used to calibrate the VSM to obtain a calibration constant.

In our experiment, we used Agilent vibrating sample magnetometer to determine the magnetization M of powder samples at room temperature.

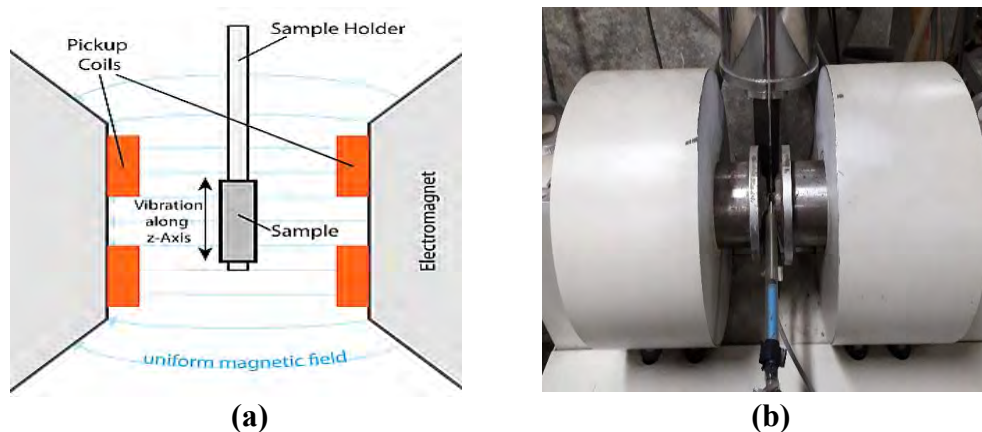


Fig. 3.3 Vibrating sample magnetometer (a) schematic and (b) experimental set-up

3.4.1.1 Calibration of vibrating sample magnetometer

We used pure Ni as a standard sample to obtain a calibration constant for magnetization measurement.

Sensitivity of VSM = $100 \mu\text{V}$,

Reference phase = 90° ,

Time constant of VSM = 30 ms,

Noise level of VSM = 24 dB,

Amplitude = $5 V_{PP}$,

Reference frequency = 37 Hz,

The saturation magnetization of pure nickel = 55.1 emu/g [111],

Mass of pure nickel = $39.5 \times 10^{-3} \text{ g}$,

Saturation voltage for nickel = 7 V,

Calibration constant of the VSM is = 0.31 emu/V .

4. RESULTS AND DISCUSSION

4.1 Structural Properties

4.1.1 X-ray diffraction analysis

Fig. 4.1 shows the XRD patterns of AFO and AFMO ceramics prepared by solid-state reaction technique with ball milling time 3 hours and 8 hours and sintered at 1000°C for 12 hours. The phase purity of the samples was measured using XRD with Cu K α radiation at room temperature. The diffraction peaks of the samples showed crystalline behavior in a pure perovskite structure with a rhombohedral symmetry [112]. The measurement confirms the *R-3c* phase of the particles. The XRD results of the samples are similar to that of α -Fe₂O₃ (*R-3c*) [15]. In XRD patterns, the peak at 30° indicates the presence of some non-stoichiometric aluminum oxide hydrate. Another disturbing peak is observed around 26.7° in the diffraction pattern which can be found in the transition phase as reported in the literature [30] while the transition phase is not stable [32]. In XRD patterns the positions of the peaks between the samples remained unchanged indicating that there is no change in the structure. From the peaks at $2\theta = 24.2^\circ$ (012) and 33.3° (104), the *d* values are measured and the cell parameters are calculated by the following equation [33],

$$\frac{1}{d^2} = \frac{(h^2+k^2)}{a^2} + \frac{l^2}{c^2}$$

Where *d* is the interplanar spacing of the crystal; *a* and *c* are the cell parameters; *h*, *k*, and *l* are plane indices. The calculated cell parameters of AFO, AFMO samples ball milled for 3 hours and 8 hours are given in Table 4.1. The lattice parameters are comparable to the values reported by Wang et al. [32].

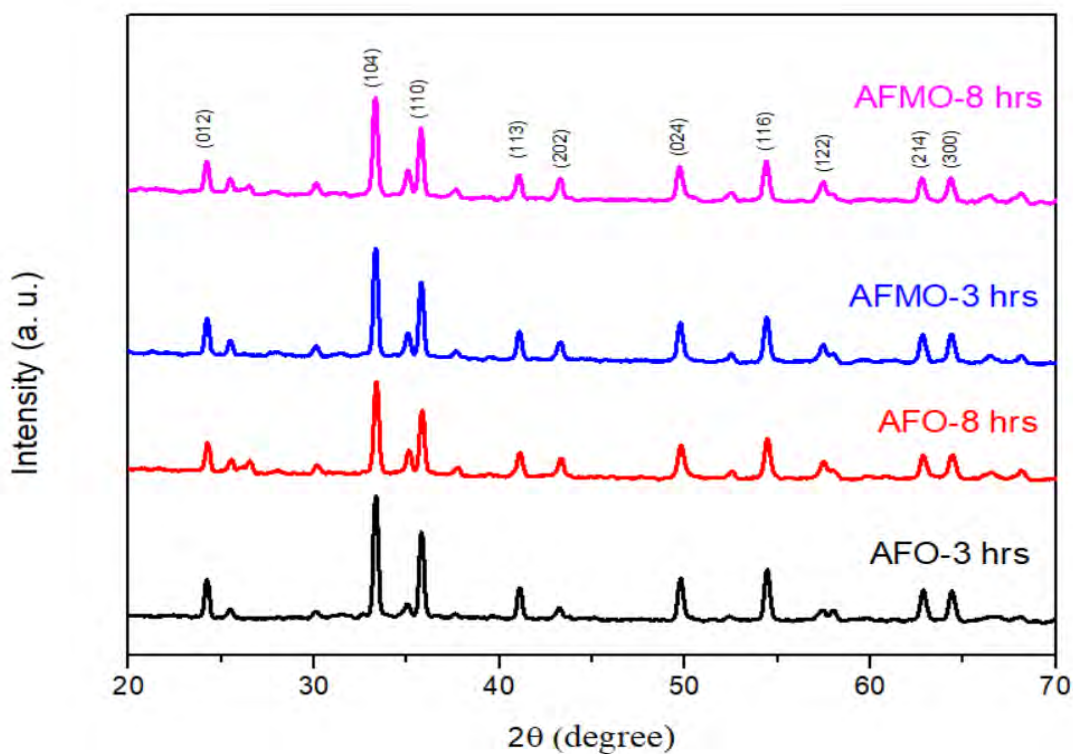


Fig. 4.1 X-ray diffraction patterns of AFO, AFMO compositions ball-milled for 3 hours and 8 hours.

Table 4.1 The crystal structure, cell parameters, volume, and crystallite size of $\text{Al}(\text{Fe}_{1-x}\text{Mn}_x)\text{O}_3$ ($x = 0.00$ and 0.02) compounds ball milled for 3 hours and 8 hours.

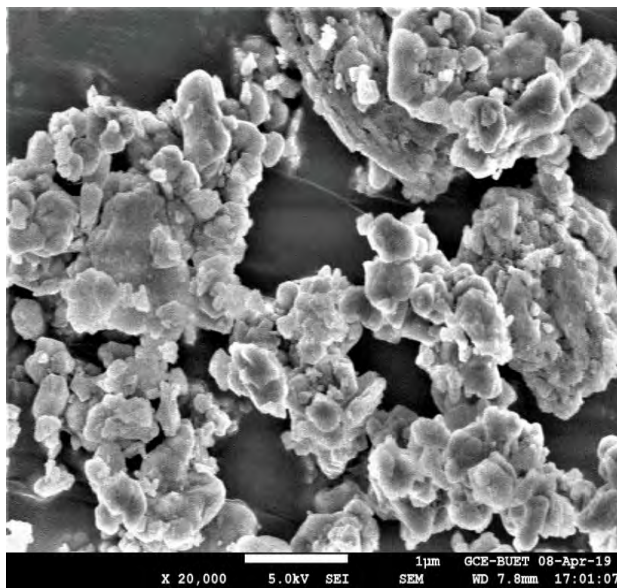
Sample name with ball milling time	Structure	cell parameters		volume (\AA^3)	angle	crystallite size (nm)
		a (\AA)	c (\AA)			
AFO- 3 hrs.	Rhombohedral	4.353	13.671	259.024	$\alpha = \beta = 90^\circ$ $\gamma = 120^\circ$	56
AFMO- 3 hrs.	Rhombohedral	4.356	13.657	259.175	$\alpha = \beta = 90^\circ$ $\gamma = 120^\circ$	53
AFO- 8 hrs.	Rhombohedral	4.334	13.693	257.195	$\alpha = \beta = 90^\circ$ $\gamma = 120^\circ$	52
AFMO- 8 hrs.	Rhombohedral	4.360	13.675	259.916	$\alpha = \beta = 90^\circ$ $\gamma = 120^\circ$	50

4.1.2 Morphological analysis

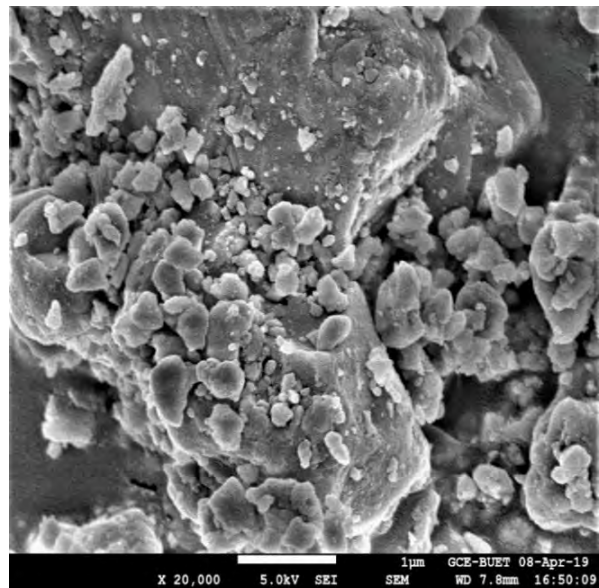
To investigate the microstructure of the surface of the powder samples, FESEM imaging was carried out for all the samples. The FESEM microstructure of the samples $\text{Al}(\text{Fe}_{1-x}\text{Mn}_x)\text{O}_3$ ($x = 0.00$ and 0.02) ball-milled for 3 hours and 8 hours and sintered at $1000\text{ }^\circ\text{C}$ are presented in Fig. 4.2 and have shown the major differences in their morphology with irregular shape. All the FESEM images in this study were taken at the same magnification of $\times 20,000$. The catalysts comprised large grains, which were embedded in a mixture consisting of small grains. It is observed from the FESEM images that the grains are segregated into different clusters. However, the size of these grains grew larger by agglomeration. Galarraga [113], indicated that high temperature could cause agglomeration of these small grains and this is also found that magnetic nanograins tend to agglomerate due to dipole-dipole magnetic interactions [114]. FESEM observations depict several agglomerations of particles. It may be due to this reason that the catalyst surface is covered with small crystallite of iron oxide, in agreement with XRD results. The aggregation effect is more significant in Fig. 4.2 (b) and from Fig. 4.2 (a) it is observed that this material has less dense and the grains are segregated into different clusters. The grains are non-uniform with varying sizes and the average grain size of the samples is varying from 183 to 320 nm. The average grain size was calculated by the linear intercept technique. The microstructural investigation revealed that Mn doping produced an increase in grain size. In Fig. 4.2 (c) and 4.2 (d), the reduction of agglomeration in Mn-doped particles is observed. There is an effect of milling time on the grain size of the particles. The grain size of the particles was reduced by increasing the ball milling time.

Table 4.2 Grain size of the compositions AFO, AFMO ball milled for 3 hours and 8 hours.

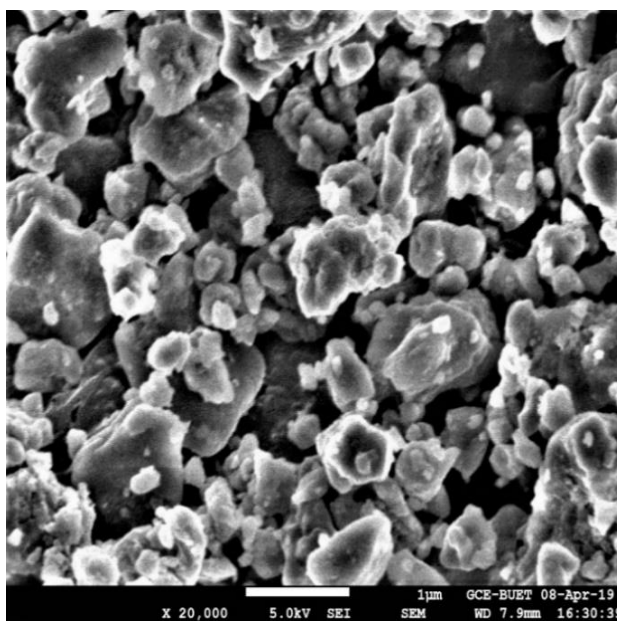
Sample name with ball milling time	AFO- 3 hrs.	AFMO-3 hrs.	AFO- 8 hrs.	AFMO-8 hrs.
Grain size (nm)	207	320	184	284



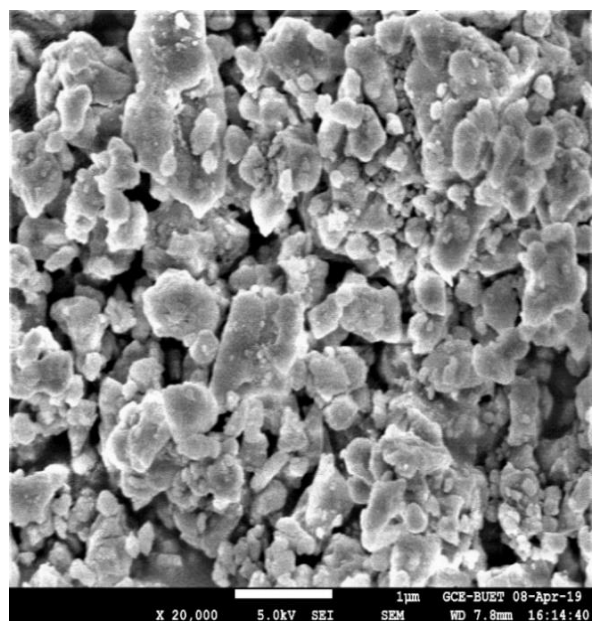
(a) The microstructure of AFO ball milled for 3 hours.



(b) The microstructure of AFO ball milled for 8 hours.



(c) The microstructure of AFMO ball milled for 3 hours.



(d) The microstructure of AFMO ball milled for 8 hours.

Fig. 4.2 The microstructure of AFO, AFMO compositions ball-milled for 3 hours and 8 hours.

4.2 AC Electrical Properties

After microstructural analysis, the AC electrical and magnetic properties of the samples are studied by impedance spectroscopy in AC electric and magnetic fields.

The disc-shaped pellets with 1 mm thickness and 13 mm in diameter are coated with a silver paste to measure the AC electrical properties of AFO, AFMO compositions ball milled for 3 hours and 8 hours at room temperature.

4.2.1 The real part of dielectric constant

Fig. 4.3 shows the Frequency-dependent Real part of the dielectric constant of AFO, AFMO-compositions ball-milled for 3 hours and 8 hours. It can be seen from Fig. 4.3 that all the samples display a decreasing trend in ϵ' with increasing frequency. This observation can be explained by the phenomenon of the dipole relaxation process. The dipoles can follow the frequency of the applied field at low frequencies, while they are incapable of following the frequency of the applied field at high frequencies [115]. Also at low-frequencies different types of polarization (dipolar, interfacial, ionic, electric) contribute to the dielectric constant. But as the frequency increases beyond a certain limit, dipoles are not being able to align themselves with the applied electric field and the contribution from different polarizations ceases. Only electronic polarization has a significant contribution to the dielectric constant at a higher frequency and subsequently the dielectric constant decreases.

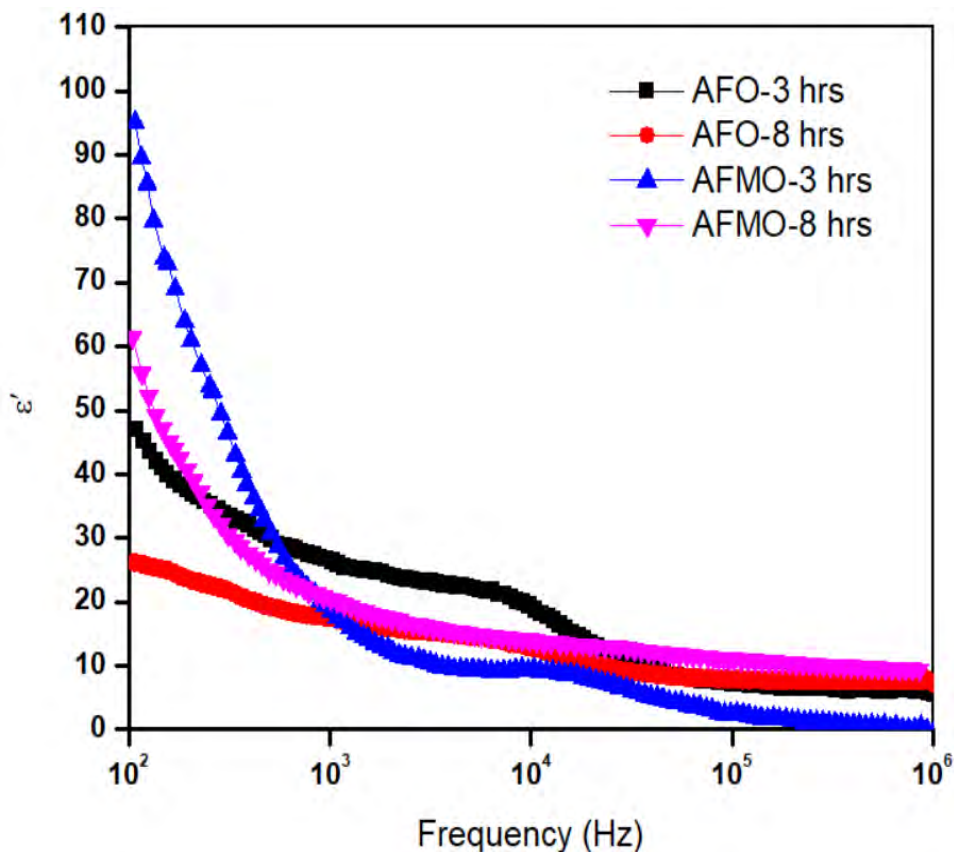


Fig. 4.3 Frequency-dependent real part of the dielectric constant of AFO, AFMO compositions ball-milled for 3 hours and 8 hours.

According to the Koops model, the dispersion observed in the dielectric constant is due to the response of electrons with the applied electric field under a certain time constraint with the alternating applied field [116]. Accordingly, the dielectric structure of a material is made up of a well-conducting layer of grains followed by a poorly conducting layer of grain boundaries. The polarization mechanism involves the exchange of electrons between the ions of the same elements, which are present in more than one valence state and are distributed randomly over crystallographic equivalent sites. During the exchange mechanism, the electrons have to pass through the grains and grain boundaries of the dielectric medium. Owing to the high resistance of the grain boundary, the electrons accumulate at the grain boundary and produce space charge polarization. It is well known that the grain boundaries are more effective at low frequency and grains are effective at high frequency [117, 118]. Hence, due to the grain boundary affect the dielectric constant decreases rapidly in the low-frequency region.

So, the decrease in dielectric constant with the increase in frequency is due to the reduction of space charge polarization. However, at low frequency, the dielectric constant was high. This is due to the presence of space charge polarization at the grain boundaries, which generates a potential barrier. Then, an accumulation of charge at the grain boundary occurred, which led to higher values of the real part of permittivity.

4.2.2 The imaginary part of dielectric constant

Fig. 4.4 shows the variation of the imaginary part of the dielectric constant (ϵ'') with frequency for the compositions AFO, AFMO ball milled for 3 hours and 8 hours, which shows similar behavior as a real part of dielectric constant. It is observed that ϵ'' decreases with the increase in frequency. As shown in Fig. 4.2, there is a linear relation between ϵ'' and frequency f , which demonstrated that conduction played an overwhelming role in dielectric dissipation. With the increase of frequency, the energy loss was gradually dominated by polarizing dipoles rather than the conduction electrons, so the permittivity exhibited the relaxation characteristics [119]. At lower frequencies, the values of the imaginary part of dielectric constant for Mn-doped samples, AFMO ball milled for 3 hours and 8 hours are higher than the Mn undoped samples. It is maybe due to the crystallite size variation effect between the samples. The crystallite size of Mn-doped samples is lower than the Mn undoped samples.

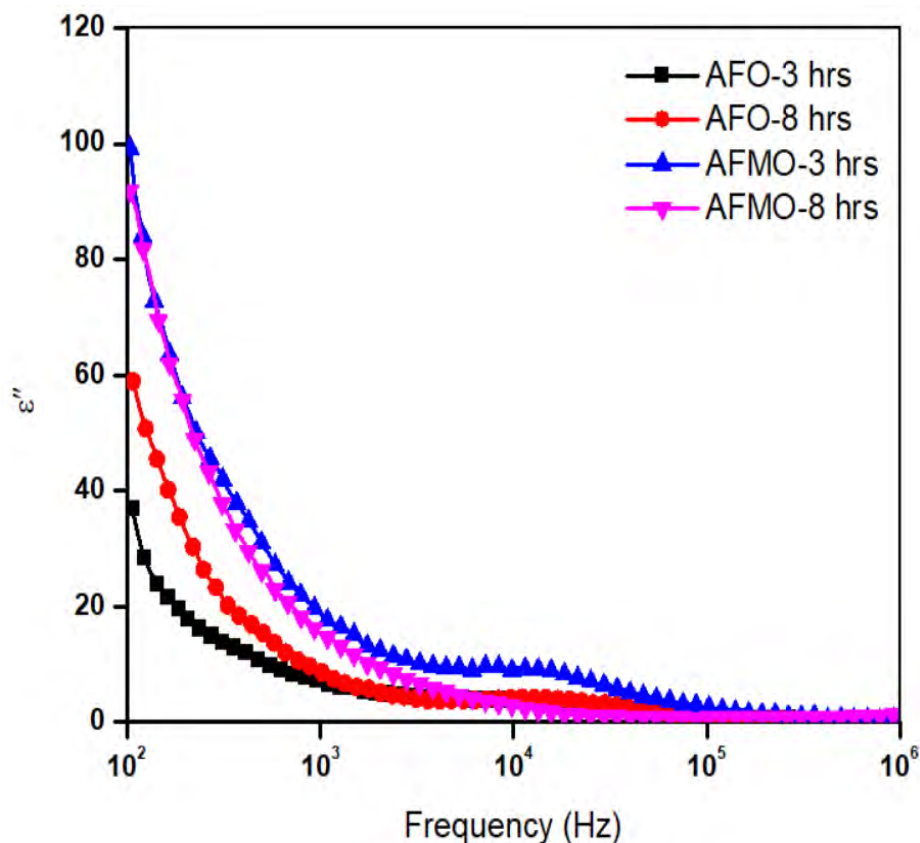


Fig. 4.4 Frequency-dependent imaginary part of the dielectric constant of AFO, AFMO compositions ball-milled for 3 hours and 8 hours.

4.2.3 Dielectric loss

Fig. 4.5 shows the frequency-dependent dielectric loss ($\tan\delta$) of AFO, AFMO compounds ball milled for 3 hours and 8 hours, measured at room temperature. The value of $\tan\delta$ denotes the dissipation of energy in the dielectric system. From Fig. 4.5, it can be seen that for all the samples there is a peak. The peak of the sample AFMO-8 hours takes place at a higher frequency which may be due to the phase transition effect. Peaks indicate the dielectric relaxation behavior of the compositions. The loss factor is attributed to domain wall resonance. At higher frequencies, the dielectric loss is low due to the inhibition of domain wall motion. The maximum dielectric loss is observed when the hopping frequency of electrons between different ionic sites becomes nearly equal to the frequency of the applied field [120]. The variation of $\tan\delta$ with frequency for all the samples indicates a gradual drop of $\tan\delta$ with the increase in frequency. The variation of dielectric loss between the samples may be due to their crystallite size variation effect.

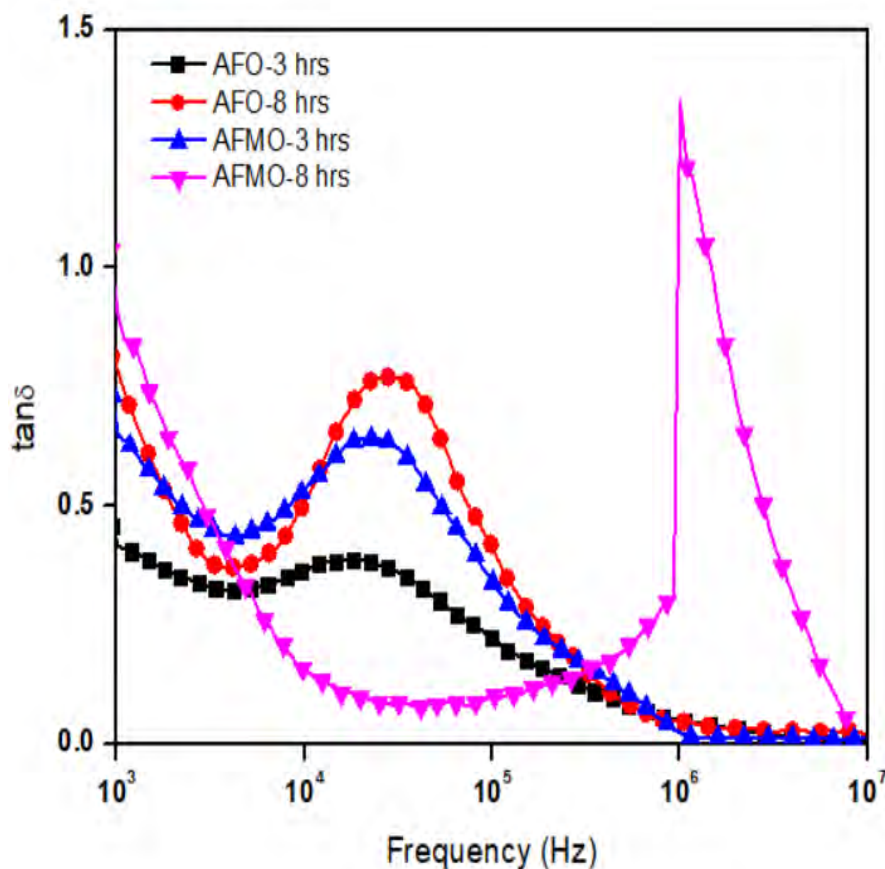


Fig. 4.5 Frequency-dependent dielectric loss of AFO, AFMO compositions ball-milled for 3 hours and 8 hours.

Fig. 4.5 implies that the hopping of charge carriers plays an important role in their transport process because a loss peak is an essential feature for charge carrier hopping transport [121]. The monotonous increase of the loss factors at low frequency is probably due to the contribution of DC conductivity [122].

4.2.4 Impedance

Fig. 4.6 shows the variation of impedance (Z) as a function of frequency for AFO, AFMO compositions ball milled for 3 hours and 8 hours. It is observed that the value of Z decreases with the increase in frequency. The decrease in Z can be attributed to the increase in conduction mechanism due to the hopping of electrons, which increases with

the increasing frequency of the applied field [123]. The decreasing value of Z indicates the loss in the resistive property of the samples. Such behavior is expected due to the presence of space charge polarization in the material. The merger of Z at a higher frequency is ascribed to the release of space charges. We also observed that there is a crystallite size effect on the variation of Z values between the samples at low frequency.

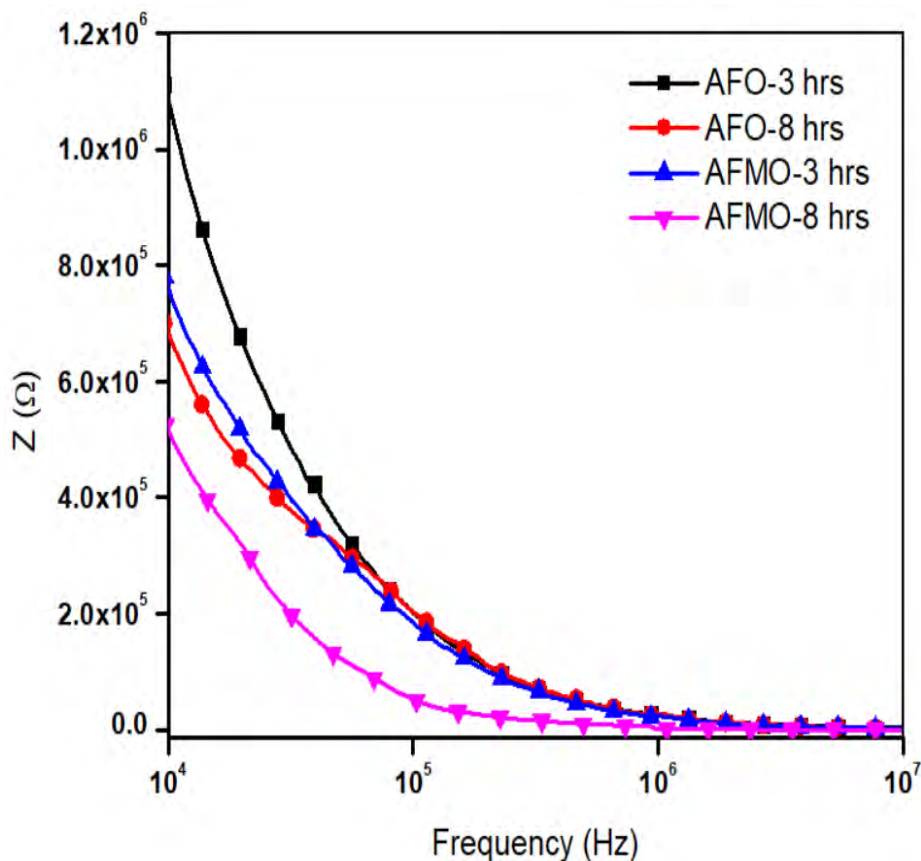


Fig. 4.6 Z as a function of frequency for AFO, AFMO compositions ball-milled for 3 hours and 8 hours.

In the measured frequency range (10^4 to 10^7 Hz), the dielectric response is dominated by relaxation phenomena because of the displacement of trapped space charges at the interfaces (Maxwell–Wagner–Sillars relaxation) [124]. Using this technique, the system can resemble mathematically an equivalent circuit, where the real part referring to loading transfer or polarization and electrode resistance is represented by resistors, and

the complex component is given by capacitance. Therefore, the impedance $Z(\omega)$ is defined as follows:

$$Z(\omega) = R(\omega) + X(\omega)$$

Where $R(\omega)$ is the resistance and $X(\omega)$ is the reactance which is related to capacitance; the conductance $C(\omega)$ is the inverse of $R(\omega)$. The frequency dependence of the impedance Z : at low frequency, the impedance is very large, because the capacitive reactance $1/\omega C$ is large. At high frequency, the capacitive reactance goes to zero (the capacitor doesn't have time to charge up) so the impedance goes to R . At the angular frequency $\omega = \omega_0 = 1/RC$, the capacitive reactance $1/\omega C$ equals the resistance R . The characteristic frequency at which Z becomes constant is called “relaxation frequency”. The ac impedance analysis is a powerful tool to separate the grain boundary and grain-electrode effects, which usually are the sites of trap for oxygen vacancies and other defects [125]. It is also useful in establishing space charge polarization and its relaxation mechanism, by aptly assigning different values of resistance and capacitance to the grain and grain boundary effects. A remarkable aspect of the impedance analysis is the option of calculating the different contributions to the conductivity, namely the bulk, grain boundary, and grain-electrode contributions. From the plots, it is seen that Z decreases monotonically with increasing frequency up to a certain limiting range ($\sim 10^6$ Hz) above which it becomes almost frequency-independent. The higher values of Z at a lower frequency indicate that the polarization in the test material is larger. This also signifies that the resistive grain boundaries become conducting at room temperature.

4.3 AC Magnetic Properties

4.3.1 The real part of permeability

Fig. 4.7 shows a representative complex permeability spectrum. From Fig. 4.7, at a low-frequency regime, initially, μ' is found to increase slightly and then remain constant for all the samples. Higher values of μ' were observed for the samples ball milled for 3 hours compared to the samples ball milled for 8 hours. The permeability in a material originates from two different magnetizing mechanisms such as spin rotation and domain wall motion, which can be described by the equation, $\mu = 1 + \chi_{\text{spin}} + \chi_{\text{dw}}$ as reported in the literature [126]. Hence the initial increase of μ' may be attributed to the combined

effect of magnetic dipolar orientations (domain wall motions) and spin rotation. The materials with homogeneous grains show higher values of permeability than materials with inhomogeneous grains. An almost constant small value of μ' is observed for the samples ball milled for 8 hrs. in the dispersion of μ' , which may originate from the rotation of spins only. Constant μ' values over a large frequency range show the compositional stability prepared by solid-state reaction [127].

From Fig. 4.8, it is observed that μ' remains almost constant with the increase of frequency and finally, a sudden drop in μ' is noticed at frequency after 10^7 Hz for all the samples at temperature 77 K. Almost constancy of μ' between 10^3 Hz to 10^7 Hz may correspond to the spin only contribution as explained in the literature [128]. However, the sudden falls of μ' in the high-frequency regime exhibit anomalous behavior and are assumed to originate from the damping mechanism of spins under the influence of applied ac magnetic field.

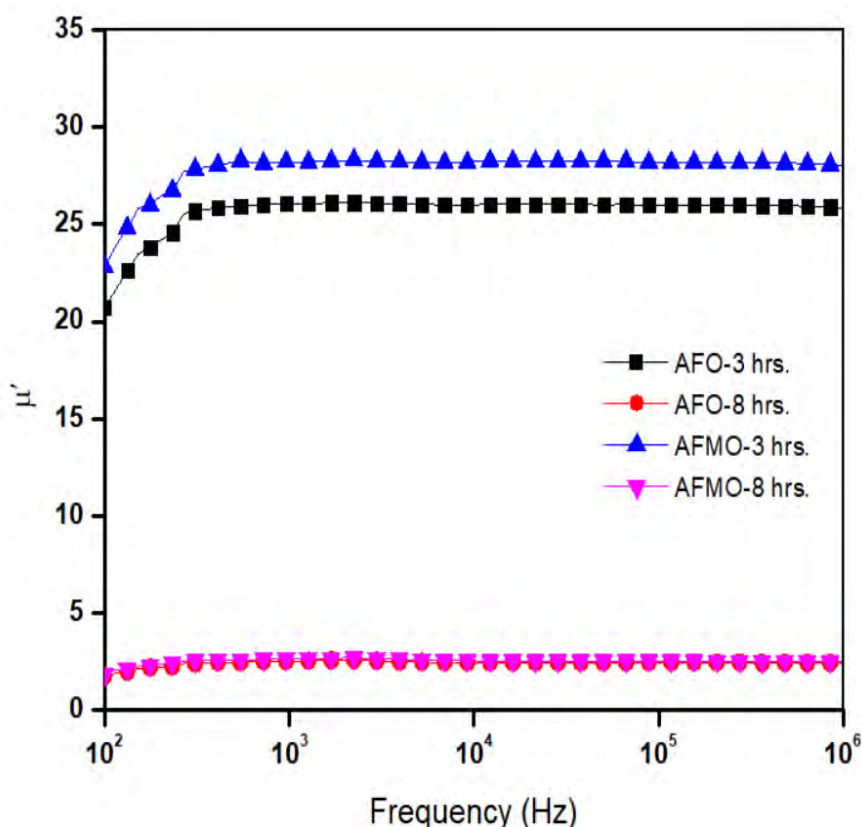


Fig. 4.7 Variation of the real part of relative permeability with the frequency of AFO, AFMO compositions ball-milled for 3 hours and 8 hours measured at room temperature.

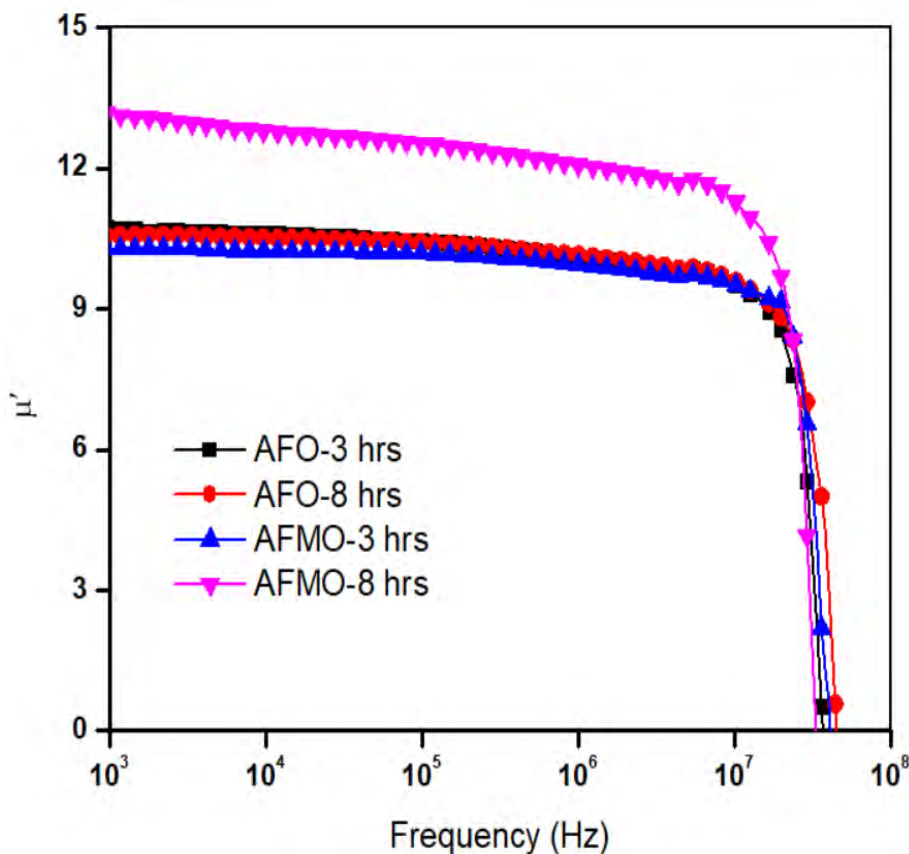


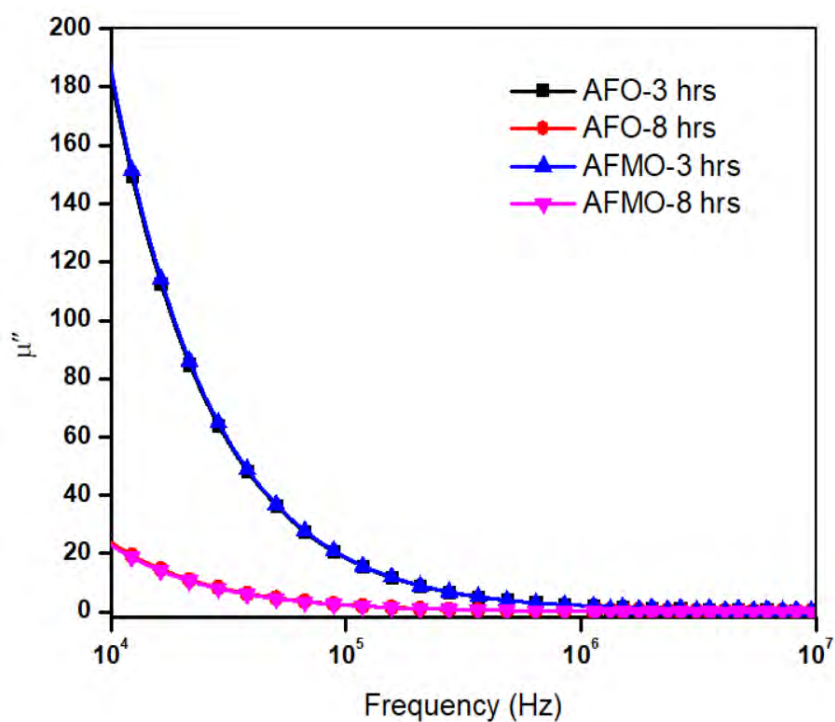
Fig. 4.8 Variation of the real part of relative permeability with the frequency of AFO, AFMO compositions ball-milled for 3 hours and 8 hours measured at temperature 77 K.

4.3.2 The imaginary part of permeability

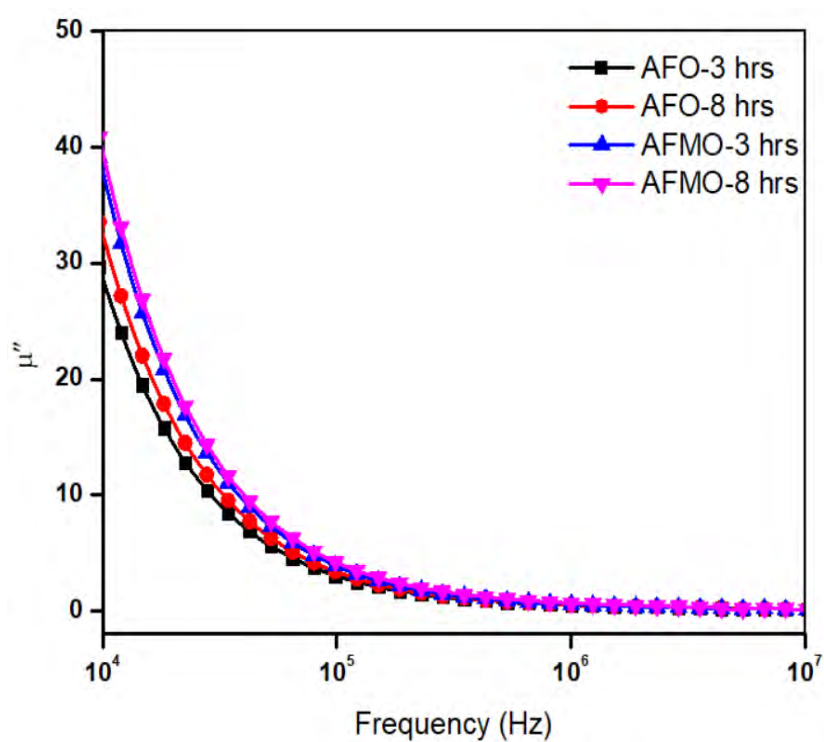
Fig. 4.9 (a) and 4.9 (b) are showing the frequency-dependent imaginary part of relative permeability (μ'') for all the samples measured at room temperature and temperature 77 K respectively. From Fig. 4.9 (a), at room temperature, it is seen almost a sharp decrease of μ'' below 10^5 Hz in their dispersion for the samples ball milled for 3 hours. This behavior of μ'' assumes to be originated from the damping of dipolar orientation (domain wall motion) because of lagging in frequency and finally above 10^6 Hz, it becomes nonresponsive to the applied magnetic field as explained in the literature [129]. The imaginary permeability decreases up to 10^6 Hz and then remains constant which indicates that the domain wall relaxation continues up to 10^6 Hz, then becomes independent of frequency. Hence, the imaginary part μ'' of AC permeability is found to be decreased with the increase in frequency due to a decrease of domain wall motion and finally, it becomes almost independent of frequency which arises from the spin-only

orientations. The behavior of μ'' may be attributed to the possible size-effect of the magnetic particles whose magnetic moments resonate well at the higher frequency regime but remain nonresponsive in the lower frequency regime. It can be mentioned that the magnetic moment of a particle is strongly size-dependent as their response to external frequency. It is assumed that as the samples are ball milled for different time durations, not every element is reduced to a certain minimum. Therefore, it can be expected that the magnetic elements in the compositions have a certain critical size distribution and have responded to the specific frequency band.

At temperature 77 K, in the low-frequency region, the imaginary part μ'' shows dispersion behaviors for all the samples, which are attributed due to the domain wall displacements. Here imaginary part μ'' decreases with increasing frequency and at higher frequency μ'' is almost independent of frequency. The frequency independence of μ'' at a higher frequency region indicates the only effectiveness of spin rotation.



(a)



(b)

Fig. 4.9 Variation of the imaginary part of relative permeability with the frequency of AFO, AFMO compositions ball-milled for 3 hours and 8 hours (a) at room temperature, (b) at temperature 77 K.

4.3.3 Magnetic loss

Fig. 4.10 and 4.11 are showing the frequency-dependent magnetic loss ($\tan\delta_M$) for all samples measured at room temperature and temperature 77 K respectively. It is seen that the value of $\tan\delta_M$ decreases exponentially with increasing frequency. The value of $\tan\delta_M$ remains almost constant showing frequency-independent behavior at a higher frequency. The $\tan\delta_M$ arises due to the lag of domain wall motion concerning the applied field and creates imperfections in the lattice. At room temperature, the value of $\tan\delta_M$ decreases for the Mn-doped sample ball milled for 8 hours due to the reduction of imperfections.

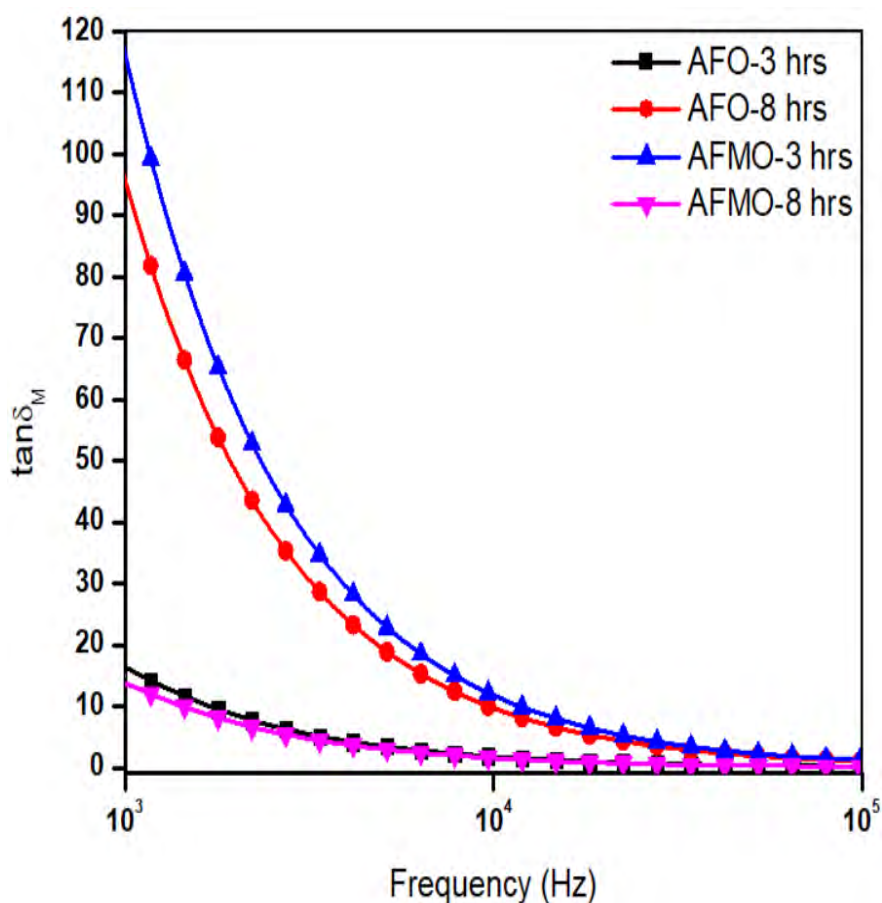


Fig. 4.10 Frequency-dependent magnetic loss of AFO, AFMO compositions ball-milled for 3 hours and 8 hours and measured at room temperature.

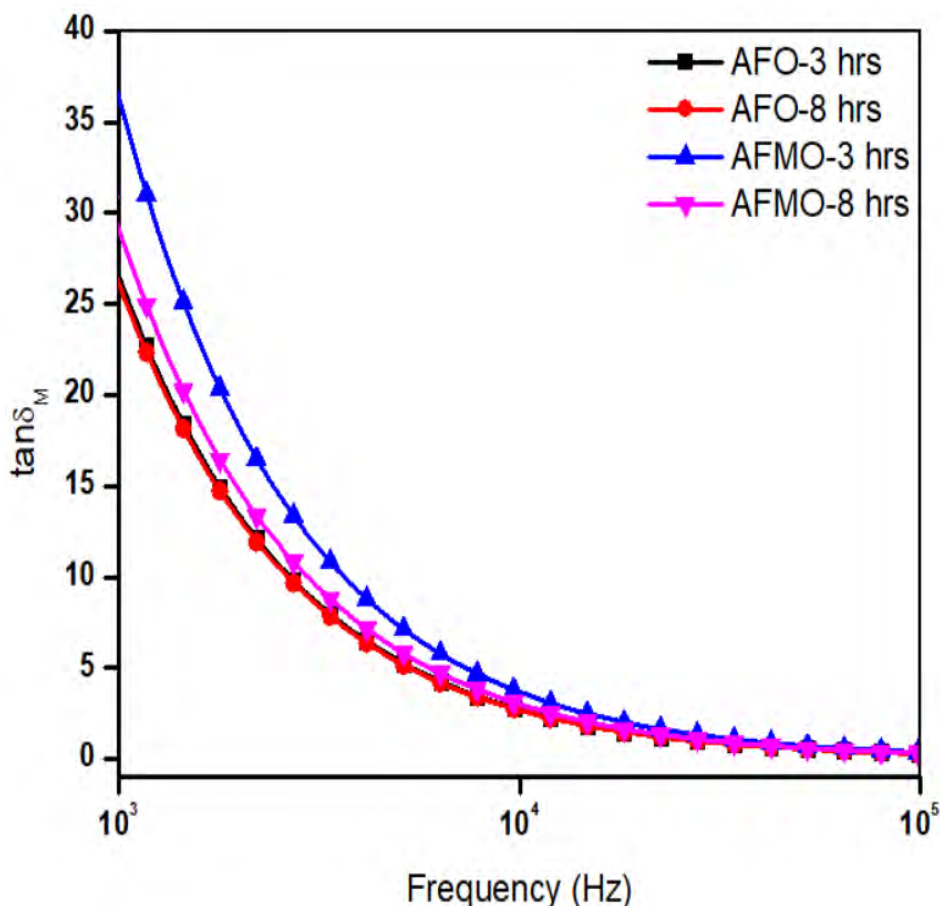


Fig. 4.11 Frequency-dependent magnetic loss of AFO, AFMO compositions ball-milled for 3 hours and 8 hours and measured at temperature 77 K.

4.3.4 Magnetic modulus

4.3.4.1 The real part of magnetic modulus

The complex permeability, in particular, the value of μ' , depends on stoichiometry, average grain size, composition, impurity, coercivity, and porosity, etc. [130, 131]. Hence, to understand and analyze the effect of milling time and Mn content on the complex permeability of the investigated samples the magnetic modulus has been used to separate the local behavior of defects from any other effects (air gap, etc.). The magnetic modulus has been determined by the usual formula from the measured values of μ' and μ'' . This formalism also provides information about inductance and magnetic resistance. This formalism also provides information about inductance and magnetic resistance. The formalisms used for estimation of both the real and imaginary part of

magnetic modulus are expressed as $M_m' = \frac{\mu'}{\mu'^2 + \mu''^2}$ and $M_m'' = \frac{\mu''}{\mu'^2 + \mu''^2}$, where, μ' is the real part and μ'' is the imaginary part of permeability [132, 133].

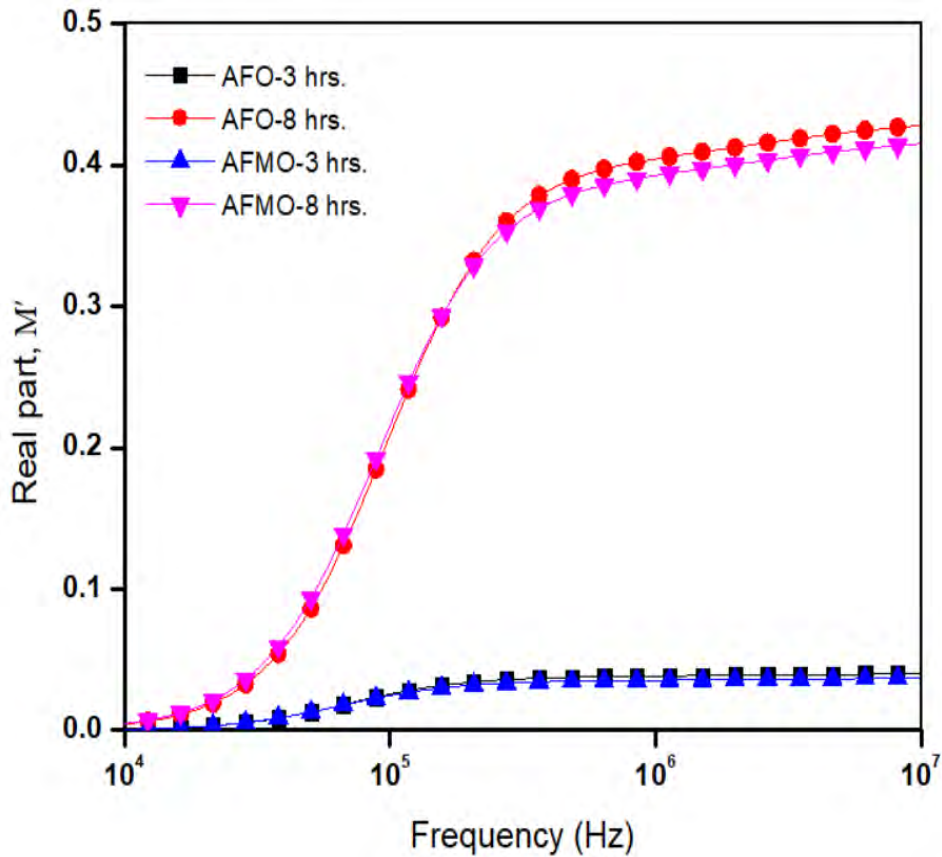


Fig. 4.12 Variation of the real part of magnetic modulus with the frequency of AFO, AFMO compositions ball-milled for 3 hours and 8 hours and measured at room temperature.

Fig. 4.12 shows the variation of the real part of magnetic modulus as a function of the frequency of the applied ac field for the investigated samples at room temperature (300K). Their real part M_m' is found to approach zero value which confirms the absence of external effects like eddy current loss due to the air gap in the coil, etc. The value of M_m' for the investigated samples increases non-linearly (almost exponentially) with the increased frequency of the applied ac field up to a certain plateau and then becomes almost independent at a single asymptotic value. The non-linear increase in M_m' is expected to be caused by both the wall motion and spin rotations [133]. However, the constancy in the real part M_m' may be produced due to the presence of spin rotations

only in the direction of the applied ac field in the grains because the dipolar orientations could not follow the frequency of the applied ac field in the high-frequency regime. As seen in Fig. 4.12, the dispersion in M_m' up to around 10 kHz remains the same for all the samples and afterward, M_m' predominantly increases for the samples ball milled for 8 hours with the increase in frequency as compared to that for the samples ball milled for 3 hours. This implies that there is more lagging between the frequency of dipolar orientations and the frequency of the applied ac field increasing the damping of wall motion. A bifurcation at around 10 kHz is observed in the dispersion of M_m' between the samples ball milled for 8 hours and ball milled for 3 hours. The lagging difference is the origin of this bifurcation in the dispersion. In this case, the real part M_m' lags more for the samples ball milled for 3 hours as compared to that for the samples ball milled for 8 hours and results in the decrease in M_m' for the samples ball milled for 3 hours.

4.3.4.2 The imaginary part of magnetic modulus

Fig. 4.13 shows the dispersion/absorption of the imaginary part M_m'' of the magnetic modulus as a function of frequency on a logarithmic scale. The well-resolved peaks are observed in their dispersion/absorption. These peaks imply the resonance effect of the dipolar and spin rotations. The frequency corresponding to each peak is termed as characteristic frequency f_{max} . The f_{max} is marked to shift rightward i.e. towards the higher frequencies for the samples with the increased milling time as seen in Fig. 4.13. The increasing rate of the magnitude of the imaginary part M'' is higher for the samples ball milled for 8 hours in comparison to the samples ball milled for 3 hours. This fact implies the more absorption of magnetic energy from the magnetic field that in turn leads to decreased spin rotations. The relaxation time constant (τ_{max}) has been estimated by using the usual formula $\tau_{max} = 1/2\pi f_{max}$ to understand the magnetic relaxation. Both f_{max} and τ_{max} for the samples AFO-3 hours, AFO-8 hours, AFMO-3 hours, and AFMO-8 hours are listed in Table 4.3.

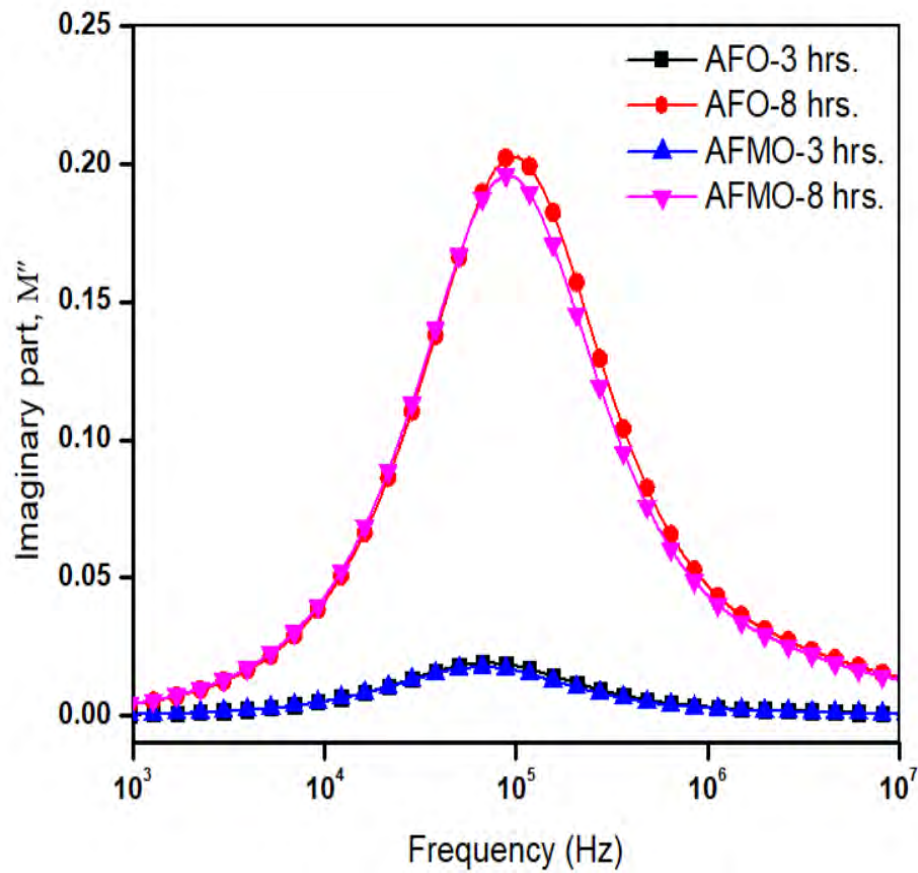


Fig. 4.13 Variation of the imaginary part of magnetic modulus with the frequency of measured AFO, AFMO compositions ball-milled for 3 hours and 8 hours measured at room temperature.

Table 4.3 f_{max} and τ_{max} for the samples AFO-3 hrs., AFO-8 hrs., AFMO-3 hrs., and AFMO-8 hrs.

Sample name with ball milling time	AFO-3 hrs.	AFO-8 hrs.	AFMO-3 hrs.	AFMO-8 hrs.
f_{max} (KHz)	66.78	102.07	66.78	88.61
τ_{max} (μ s)	2.38	1.56	2.38	1.8

From Table 4.3, it is seen that the relaxation time constant τ_{max} has decreased for the samples ball milled for 8 hours. This signifies the increase in the damping mechanism of wall motion that causes a decrease in the permeability of the material.

4.3.4.3 Nyquist plot of magnetic modulus

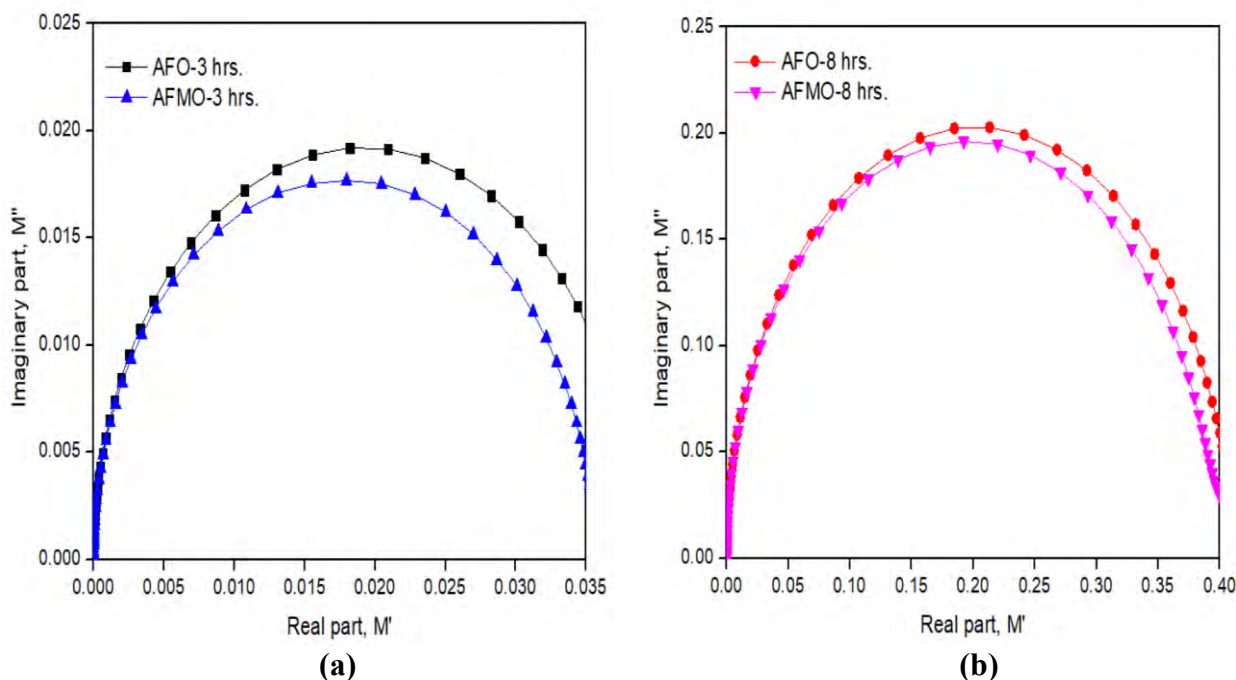


Fig. 4.14 Nyquist plot for (a) AFO, AFMO compositions ball-milled for 3 hours and (b) AFO, AFMO compositions ball-milled for 8 hours and measured at room temperature.

The single semicircle is observed for the samples in their Nyquist plot as shown in Fig. 4.14 and therefore represents a single time constant of magnetic relaxation, in particular, spin relaxation across their grain boundaries. In the low-frequency region, the non-zero value of the imaginary part M'' indicates that both the wall resonance and resonance rotations (spin resonance) contribute to their permeability [133]. However, the wall resonance gradually damped with the increase in applied frequency, and finally, only the resonance rotation plays its role to increase their permeability to a single asymptotic value. Moreover, each semicircle corresponds to each composition that may be fitted to an equivalent circuit comprising of an inductance and a resistance in series combination [133].

4.4 DC Magnetic Properties

The DC magnetic property measurements for AFO, AFMO compositions, ball milled for 3 hours and 8 hours are taken at room temperature.

To observe the magnetic ordering in AFO, AFMO compositions ball milled for 3 hours and 8 hours, the dc-magnetization measurements have been carried out as a function of the applied magnetic field by using a vibrating sample magnetometer at room temperature as shown in Fig. 4.15 and Fig. 4.16. In the DC magnetic measurements at room temperature (298 K), all the samples are showing unsaturated high values of magnetization which confirm the antiferromagnetic nature of the compounds. The increasing rate of magnetization for all the samples is higher at the lower magnetic field while it becomes lower at the higher magnetic field by remaining unsaturated. The DC magnetic measurements suggest the classical spin-glass behavior of the compositions for their magnetically frustrated systems. Magnetically frustrated systems have been identified to possess the ME effect at low temperatures.

Fig. 4.15 and Fig. 4.16 are representing the Effect of Mn doping on the M-H loop of AFO, AFMO compositions ball-milled for 3 hours and 8 hours. When Fe^{3+} ions in AFO are replaced by 2% Mn^{2+} ions, the magnetization appears to be affected by the contribution of Mn^{2+} . Therefore, the antiferromagnetic coupling among Fe ions (or Mn ions) is enhanced by the Mn substitution.

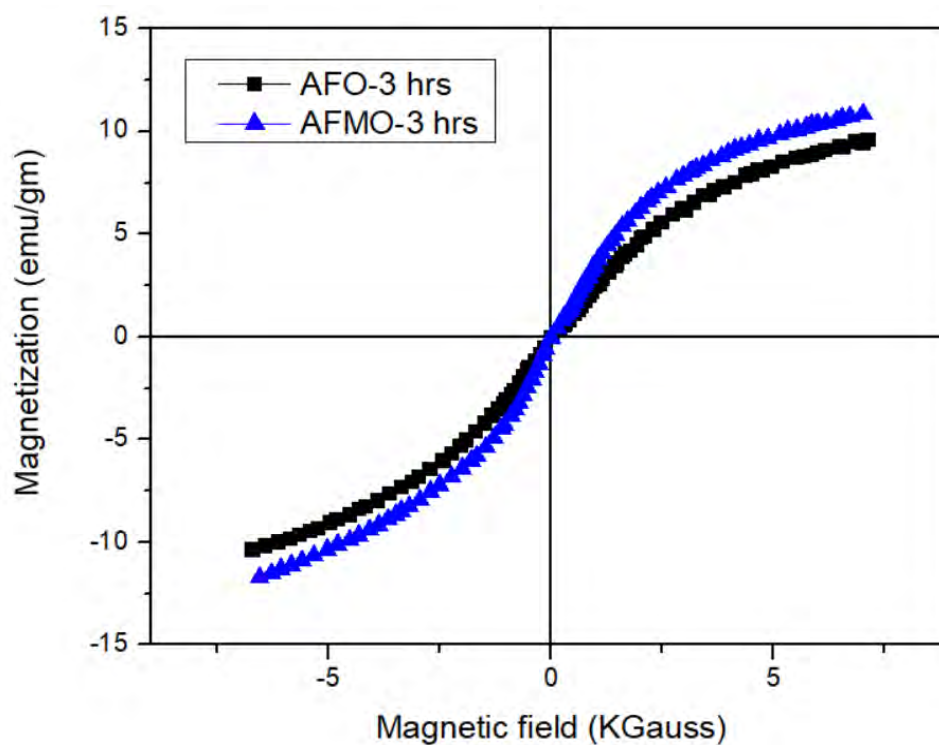


Fig. 4.15 M-H loop of AFO, AFMO compositions ball-milled for 3 hours respectively.

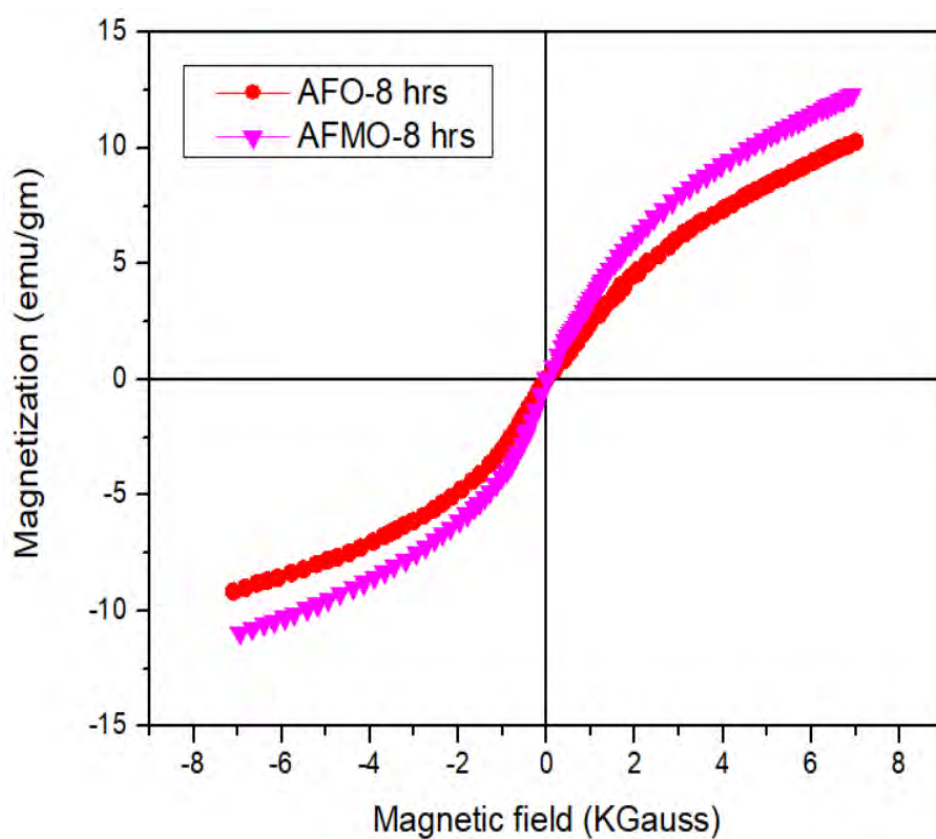


Fig. 4.16 M-H loop of AFO, AFMO compositions ball-milled for 8 hours respectively.

5. CONCLUSIONS

5.1 Summary

Polycrystalline AFO, AFMO ceramics were synthesized by solid-state reaction technique and the samples were ball milled for 3 hours and 8 hours during sample preparation. The objective of this thesis work is to observe the effect of 2% Mn doping on the Fe side and the variation of ball milling time on the structural, magnetic, and dielectric properties of AFO and Mn-doped AFO. AFO is a promising material because it exhibits antiferromagnetism and ferroelectricity in a single phase at room temperature. AFO is antiferromagnetic with no hysteresis loop. This chapter presents a summary of the results and discussion presented in the previous chapter and also suggestions for the scope of future work.

The phase purity of the samples was measured using X-ray powder diffraction. The diffraction peaks for all the samples showed crystalline behavior in rhombohedral symmetry with space group $R-3c$. There were variations in crystallite sizes among the samples due to the variation of ball milling time and the effect of Mn doping in the Fe side of AFO. The crystallite size decreases with the increase in ball milling time and also decreases with Mn doping. The crystallite size is reduced because of the lattice distortion caused by the radius difference between Mn^{2+} and Fe^{3+} . The FESEM microstructures of the samples have shown major differences in their morphology with irregular shapes. The grains are non-uniform with varying sizes and the average grain sizes are varying from 183 to 320 nm among the samples. Reduction of agglomeration is observed in Mn-doped particles. The grain size of the particles was reduced by increasing the ball milling time. All the samples display a decreasing trend in dielectric constant with increasing frequency. The decrease in dielectric constant with the increase in frequency is due to the reduction of space charge polarization. $\tan\delta$ denotes the dissipation of energy in the dielectric system. The variations of $\tan\delta$ with frequency for all the samples indicate a gradual drop of $\tan\delta$ with the increase in frequency. The loss factor is attributed to domain wall resonance. The monotonous increase in loss factor at lower frequency is probably due to the contribution of dc conductivity. At high frequency, the dielectric loss is low due to the inhibition of domain wall motion. It is observed that the value of Impedance, Z decreases with the increase in frequency for all

the samples. The decreasing rate of Z indicates the loss in resistive property of the samples and such behavior is expected due to the presence of space charge polarization in the material. It is also observed that there is a crystallite size effect on the variation of the values of Z among the samples at a lower frequency. At room temperature, in the low-frequency regime, initially, μ' is found to increase slightly and then remain constant for all the samples. The initial increase of μ' may be attributed to the combined effect of magnetic dipolar orientations and spin rotation. Higher values of μ' were observed for the samples ball milled for 3 hours compared to the samples ball milled for 8 hours. An almost constant small value of μ' is observed for the samples ball milled for 8 hrs. in the dispersion of μ' , which may originate from the rotation of spins only. Constant μ' values over a large frequency range show the compositional stability prepared by the solid-state reaction. At temperature 77 K, the real part of permeability, μ' remains almost constant with the increase in frequency and finally, a sudden drop of μ' is noticed at frequency after 10^7 Hz for all the samples. The sudden falls of μ' in the high-frequency regime exhibit anomalous behavior and are assumed to originate from the damping mechanism of spins under the influence of applied ac magnetic field. At room temperature, it is seen almost a sharp decrease in the imaginary part of permeability μ'' below 10^5 Hz in their dispersion for the samples ball milled for 3 hours. This behavior of μ'' assumes to be originated from the damping of dipolar orientation because of lagging in frequency and finally above 10^6 Hz, it becomes nonresponsive to the applied magnetic field. At 77K, in the lower frequency region, the imaginary part μ'' shows dispersion behavior which is attributed due to domain wall displacements, and in the higher frequency region, μ'' is almost independent of frequency indicating only effectiveness of spin rotation there. It is seen that the relaxation time constant τ_{max} has decreased for the samples ball milled for 8 hours. The single semicircle is observed for all the experimental samples in their Nyquist plot representing a single time constant of magnetic relaxation. The DC magnetization measurements were carried out as a function of applied magnetic field $M(H)$ by using a vibrating sample magnetometer at room temperature. In this measurement, all the samples show unsaturated high values of magnetization which confirms the antiferromagnetic nature of the compounds suggesting the classical spin-glass behavior of the compositions for their magnetically frustrated systems. Magnetization is observed to be increased with Mn doping in the Fe side of AFO.

5.2 Suggestions for Future Work

Further studies on different aspects are possible for the fundamental interest of the studied materials.

1. Mössbauer spectroscopy can be performed to know the cation distribution and oxidation state of iron.
2. Raman spectroscopy of the compositions can be studied to measure bond length, bond angle, etc.

References

- [1] Hill, N. A., “Why are there so few magnetic ferroelectrics?”, *J. Phys. Chem. B*, Vol. 104 (29), pp. 6694-6709, 2000.
- [2] Rao, C. N. R., Sundaresan, A., and Saha, R., “Multiferroic and magnetoelectric oxides: The emerging scenario,” *J. Phys. Chem. Lett.*, Vol. 3, pp. 2237-2246, 2012.
- [3] Saha, R., Sundaresan, A., and Rao, C. N. R., “Novel features of multiferroics and magnetoelectric ferrites and chromites exhibiting magnetically driven ferroelectricity,” *Mater. Horiz.*, Vol. 1, pp. 20-31, 2014.
- [4] Bousquet, E., Dawber, M., Stucki, M., Lichtensteiger, C., Hermet, P., Gariglio, S., Triscone, J. M., and Ghosez, P., “Improper ferroelectricity in perovskite oxide artificial superlattices”, *Nature*, Vol. 452, pp.732-736, 2008.
- [5] Suntivich, J., May, K. J., Gasteiger, H. G., Goodenough, J. B., and Shao-Horn Y., “A perovskite oxide optimized for oxygen evolution catalysis from molecular orbital principles”, *Science*, Vol. 334, pp. 1383-1385, 2011.
- [6] Kozuka, Y., Kim, M., Bell, C., Kim, Bog G., Hikita, Y., and Hwang, H. Y., “Two-dimensional normal-state quantum oscillations in a superconducting heterostructure”, *Nature*, Vol. 462, pp. 487-490, 2009.
- [7] Benedek, N. A., and Fennie, C. J., “Hybrid improper ferroelectricity: A mechanism for controllable polarization-magnetization coupling”, *Phys. Rev. Lett.*, Vol. 106, pp. 107204-4, 2011.
- [8] Kim, W., We, J. H., Kim, S. J., Kim, C. S., “Effect of cation distribution for $AFeO_3$ ($A = Ga, Al$)”, *J Appl. Phys.*, 101:09M515–509M515, 2007.
- [9] Schieber, M., Frankel, R. B., Blum, N. A., Foner, S., “High-magnetic-field studies of orthorhombic and rhombohedral $Al_{2-x}Fe_xO_3$ compounds”, *J. Appl. Phys.*, Vol. 38, pp. 1282-1283, 1967.
- [10] Saha, R., Shireen, A., Shirodkar, S. N., Waghmare, U. V., A. Sundaresan, A., and Rao, C. N. R., “Multiferroic and magnetoelectric nature of $GaFeO_3$, $AlFeO_3$ and related oxides,” *Solid State Commun.*, Vol. 152, pp. 1964-1968, 2012.
- [11] Saha, R., Shireen, A., Mandal, P., Sundaresan, A., and Rao, C. N. R., “Multiferroic and magnetodielectric properties of the $Al_{1-x}Ga_xFeO_3$ family of oxides,” *J. Mater. Chem.*, Vol. 152, pp. 1964-1968, 2011.
- [12] Villafuerte-Castrejón, M. E., Castillo-Pereyra, E., Tartaj, J., Fuentes, L., Bueno-Baqués, D., González, G., Matutes-Aquino, J. A., *J. Magn. Magn. Mater.*, 272-276: 837–839.
- [13] Trooster, J., Dymanus, A., “Mössbauer effect in $Ga_{2-x}Fe_xO_3$ and related

- compounds”, *Phys. Status Solidi B*, Vol. 24, pp. 487–499, 1967.
- [14] Yuan, Z. H., Wang, Y. H., Sun, Y. C., Wang, J., Bie, L. J., Duan, Y. Q., "Sunlight-activated AlFeO₃/TiO₂ photocatalyst", *Sci. China Ser.*, Vol. 49, pp. 67, 2006.
- [15] Saha, R., Shireen, A., Shirodkar, S. N., Singh, M. S., Waghmare, U. V., Sundaresan, A., and Rao, C. N. R., "Phase transitions of AlFeO₃ and GaFeO₃ from the chiral orthorhombic (Pna2₁) structure to the rhombohedral (R $\bar{3}c$) structure”, *Inorg. Chem.*, Vol. 50, pp. 9527-9532, 2011.
- [16] Santos, G. M., Silva, D. M., Freitas, V. F., Dias, G. S., Coelho, A. A., Pal, M., Santos, I. A., Cótica, L. F., Guo, R., Bhalla, A. S., "Multiferroic behavior of lead-free AlFeO₃ and Mn, Nb doped compositions”, *Ferroelectrics*, Vol. 460, pp. 108–116, 2014.
- [17] Lee, H., Choeng, S. W., and Kim, Bog G., "Hybrid functional band gap calculation of SnO₆ containing perovskites and their derived structures”, *J. Solid State Chem.* Vol. 228, pp. 214-220, 2015.
- [18] Rondinelli, J. M., and Spaldin, N. A., "Structure and properties of functional oxide thin films: Insights from electronic-structure calculations”, *Adv. Mater.*, Vol. 23, pp. 3363-81, 2011.
- [19] Malashevich, A., and Vanderbilt, D., "First-principles study of improper ferroelectricity in TbMnO₃”, *Phys. Rev. Lett.*, Vol. 101, pp. 037210-4, 2008.
- [20] Lee, J. H., and Rabe, K. M., "Coupled magnetic-ferroelectric metal-insulator transition in epitaxially strained SrCoO₃ from first principles”, *Phs. Rev. Lett.*, Vol. 107, pp. 067601-4, 2011.
- [21] Singh, S., Haraldsen, J. T., Xiong, J., Choi, E. M., Lu, P., Yi, D., Wen, X. D., Liu, J., Wang, H., Bi, Z., Yu, P., Fitzsimmons, M. R., MacManus-Driscoll, J. L., Ramesh, R., Balatsky, A. V., Zhu J. X., and Jia, Q. X., "Induced magnetization in La_{0.7}Sr_{0.3}MnO₃/BiFeO₃ superlattices”, *Phys. Rev. Lett.*, Vol. 113, pp. 047204-5, 2014.
- [22] Cótica, L. F., De Medeiros, S. N., Santos, I. A., Jr. Paesano, A., Kinast, E. J., Da Cunha, J. B. M., Venet, M., Garcia, D., Eiras, J. A., "Structural, magnetic, and dielectric investigations of the FeAlO₃ multiferroic ceramics”, *Ferroelectrics*, Vol. 338, pp. 241-246, 2006.
- [23] Cótica, L. F., Santos, I. A., Venet, M., Garcia, D., Eiras, J. A., Coelho, A. A., "Dielectric and magnetic coupling in lead-free FeAlO₃ magnetoelectric compound”, *Solid State Commun.*, Vol. 147, pp. 123-125, 2008.
- [24] Mahmood, L. S., "Preparation of Co_{1-x}Zn_xFe₂O₄ nano ferrite and study of its electrical and structural properties”, *Scientific Research University of Diyala College of Science Department of Physics*, pp. 63-64, 2012.

- [25] Kida, N., Kaneko, Y., He, J. P., Matsubara, M., Sato, H., Akoh, H. and Tokura, Y., “Enhanced optical magnetoelectric effect in a patterned polar ferrimagnet”, *Phys. Rev. Lett.*, Vol. 96, pp. 167202, 2006.
- [26] Kim, J.-Y., Koo, T. Y. and Park, J. -H., “Orbital and bonding anisotropy in a half-filled GaFeO₃ magnetoelectric ferrimagnet”, *Phys. Rev. Lett.*, Vol. 96, pp. 047205, 2006.
- [27] Arima, T., Higashiyama, D., Kaneko, Y., He, J. P., Goto, T., Miyasaka, S., Kimura, T., Oikawa, K., Kamiyama, T., Kumai, R., and Tokura, Y., “Structural and magnetoelectric properties of Ga_{2-x}Fe_xO₃ single crystals grown by a floating-zone method”, *Phys. Rev. B*, Vol. 70, pp. 064426, 2004.
- [28] Popov, Yu. F., Kadomtseva, A. M., Vorob’ev, G. P., Timofeeva, V. A., Ustinin, D. M., Zvezdin, A. K., & Tegeranchi, M. M., “Magnetoelectric effect and toroidal ordering in Ga_{2-x}Fe_xO₃”, *Journal of Experimental and Theoretical Physics*, Vol. 87, pp. 146, 1998.
- [29] Kimura, T., Goto, T., Shintani, H., Ishizaka, K., Arima, T., and Tokura, Y., “Magnetic control of ferroelectric polarization”, *Nature*, Vol. 426, pp. 55, 2003.
- [30] Tyagi, S., Sharma, G., Choudhary, R. J., and Sathe V. G., “‘Phonon invisibility’ driven by robust magneto-elastic coupling in AlFeO₃ thin film”, *J. Appl. Phys.*, 126, 085302, 2019.
- [31] Shirolkar, M. M., Li, M., and Wang, H., “Magnetic and ferroelectric properties of sol-gel synthesized rhombohedral phase AlFeO₃ nanoparticles”, *J. Phys.: Conf. Series*, Vol. 864, pp. 012009, 2017.
- [32] Li, Q., Wang, S., Yuan, Y., Gao, H., and Xiang, X., “Phase-controlled synthesis, surface morphology, and photocatalytic activity of the perovskite AlFeO₃”, *J. Sol-Gel Sci. Technol.*, 2017.
- [33] Wang, S., Zhang, C., Sun, G., Chen, B., Xiang, X., Wang, H., Fang, L., Tian, Q., Ding, Q., and Zu, X. T., “Fabrication of a novel light emission material AlFeO₃ by a modified polyacrylamide gel route and characterization of the material”, *Opt. Mater.*, Vol. 36, pp. 482–488, 2013.
- [34] Rao, B. N., Yasui, S., Katayama, T., Taguchi, A., Moriwake, H., Hamasaki, Y., and Itoh, M., “Investigation of room temperature ferroelectricity and ferrimagnetism in multiferroic Al_xFe_{2-x}O₃ epitaxial thin films”, *arXiv e-prints*, pp. arXiv-1903, 2019.
- [35] Hamasaki, Y., Shimizu, T., Taniguchi, H., Taniyama, T., Yasui S., and Itoh, M., “Epitaxial growth of metastable multiferroic AlFeO₃ film on SrTiO₃ (111),” *Appl. Phys. Lett.*, Vol. 104, pp. 082906, 2014.
- [36] Kumar, P., Bera, A., Muthu, D. V. S., Shirodkar, S. N., Saha, R., Shireen, A., Sundaresan, A., Waghmare, U. V., Sood, A. K., and Rao, C. N. R., “Coupled phonons, magnetic excitations, and ferroelectricity in AlFeO₃: Raman and first-

- principles studies”, *Phys Rev. B*, Vol. 85, pp. 134449, 2012.
- [37] Shirolkar, M. M., and Wang, H., “AlFeO₃ Nanoparticles: An efficient perovskite material for low operating bias memristive devices”, *IEEE International Conference on Nanotechnology*, pp. 493-495, 2015.
- [38] Mohamed, M. B., Fuess, H., “Effect of Mn doping on structural and magnetic properties of GaFeO₃”, *J. Magn. Magn. Mater.*, Vol. 323, pp. 2090, 2011.
- [39] Nagai, T.; Hamane, D.; Devi, P. S.; Miyajima, N.; Yagi, T.; Yamanaka, T.; Fujino, K. “A new polymorph of FeAlO₃ at high pressure”, *J. Phys. Chem. B*, Vol. 109, pp. 18226, 2005.
- [40] Bouree, F., Baudour, J. L., Elbadraoui, E., Musso, J., Laurent, C., Rousset, A., “Crystal and magnetic structure of piezoelectric, ferrimagnetic and magnetoelectric aluminum iron oxide FeAlO₃ from neutron powder diffraction”, *Acta Crystallogr. B*, Vol. 52, pp. 217-222, 1996.
- [41] Yuan, Z., Wang, Y., Sun, Y., Wang, J., Bie, L., Duan, Y., “Sunlight-activated AlFeO₃/TiO₂ photocatalyst”, *Sci. China Ser. B*, Vol. 49, pp. 67-74, 2006.
- [42] Han, T. C., Chen, T. Y., and Lee, Y. C., “Grain size effect on site-disorder and magnetic properties of multiferroic GaFeO₃ nanoparticles”, *Appl. Phys. Lett.*, Vol. 103, pp. 232405, 2013.
- [43] Brown, I. W. M., Mackenzie, K. J. D. and Cardile, C. M., “Lattice parameters and Mössbauer spectra of iron-containing corundum (α -Al₂O₃)”, *Journal of Materials Science Letters*, Vol. 6(5), pp. 535-540, 1987.
- [44] Cullity, B. D., Graham, C. D., “Introduction to magnetic materials”, *John Wiley and son's cor.*, 2nd edition, chap. 3, 2005.
- [45] Schmid, H., “Multi-ferroic magnetoelectric”, *Journal of ferroelectrics*, vol. 162, pp. 317-338, 1994.
- [46] Khomskii, D., "Trend: Classifying multiferroics: Mechanisms and effects", *Physics*, Vol.2, pp. 20, 2009.
- [47] Ramesh, R., Spaldin, N. A., "Multiferroics: progress and prospects in thin films", *Nanosci. Technol.: A Collection of Reviews from Nature Journals*, pp. 20-28, 2010.
- [48] Spaldin, N. A., "Multiferroics: from the cosmically large to the subatomically small", *Nat. Rev. Mater.*, Vol. 2 (5), pp. 1-3, 2017.
- [49] Prinz, G. A., “Magnetoelectronics”, *Science*, Vol. 282, pp. 1660-1663, 1998.
- [50] Roy, A., Gupta, R., Garg, A., “Magnetoelectric memories: A review”, *Adv. Cond. Mat. Phys.*, Article ID 926290, 2012.

- [51] Schmid, H., "On the possibility of ferromagnetic, antiferromagnetic, ferroelectric and ferroelastic domain reorientations in magnetic and electric fields", *Ferroelectrics*, Vol. 221, pp. 9-17, 1999.
- [52] Eerenstein, W., Mathur, N. D., Scott, J. F., "Multiferroic and magnetoelectric materials", *Nature*, Vol. 442, pp. 759, 2006.
- [53] Remeika, J. P., "GaFeO₃:A ferromagnetic-piezoelectric compound" *J. Appl. Phys.*, Vol. 31, S263, 1960.
- [54] Rado, G. T., "Observation and possible mechanisms of magnetoelectric effects in a ferromagnet", *Phys. Rev. Lett.*, Vol. 13, pp. 335, 1964.
- [55] Frankel, R. B., Blum, N. A., Foner, S., Freeman, A. J., Schieber, M., "Ferrimagnetic structure of magnetoelectric Ga_{2-x}Fe_xO₃", *Phys. Rev. Lett.*, Vol. 15, pp. 958-960, 1965.
- [56] Känzig, W., "Ferroelectrics and antiferroelectrics", *Solid State Phys.*, pp. 1-197, 1957.
- [57] Lines, M., and Glass, A., "Principles and applications of ferroelectrics and related materials", *Oxford university press*, 2001.
- [58] Wenk, H.-R., Bulakh, A., "Minerals: Their constitution and origin", *Cambridge University Press*, 2016.
- [59] Kanhere, P., and Chen, Z., "A review on visible light active perovskite-based photocatalysts", *Molecules*, Vol. 19, pp. 19995-20022, 2014.
- [60] Goldschmidt, V. M., Vidensk, S. N. and Oslo, A. I., "Geochemical distribution laws of the elements. VIII. Researches on the structure and properties of crystals", *Mat. Nat.*, Vol. 8, pp. 34, 1926.
- [61] Kulkarni, A., Ciacchi, F. T., Giddey, S., Munnings, C., et al., "Mixed ionic electronic conducting perovskite anode for direct carbon fuel cells", *Int. J. Hydrogen Energy*, 37(24), pp. 19092–19102, 2012.
- [62] Coey, J. M. D., Viret, M., and Molnar, S. von, "Mixed-valence manganites", *Adv. Phys.*, 48 (2), pp. 167–293, 1999.
- [63] Bhalla, A.S., Guo, R., and Roy, R., "The perovskite structure—a review of its role in ceramic science and technology", *Mat. Res. Innov.*, Vol. 4, pp. 3–26, 2000.
- [64] Tyndall, C., "Nanoscale discovery could push perovskite solar cells to 31% efficiency", *Green Energy*, 2016.
- [65] Stranks, S. D., Snaith, H. J., "Metal-halide perovskites for photovoltaic and light-emitting devices", *Nat. Nanotechnol.*, 10 (5): 391–402, 2015.
- [66] Fiebig, M., "Revival of the magnetoelectric effect", *J. Phys. D: Appl. Phys.*, Vol.

38 (8): R123, 2005.

- [67] Dziom, V., Shuvaev, A., Pimenov, A., Astakhov, G. V., Ames, C., Bendias, K., Böttcher, J., Tkachov, G., Hankiewicz, E. M., Brüne, C., and Buhmann, H., “Observation of the universal magnetoelectric effect in a 3D topological insulator”, *Nat. Commun.*, Vol. 8, pp. 1-8, 2017.
- [68] Röntgen, W.C., "Ueber die durch Bewegung eines im homogenen electrischen Felde befindlichen Dielectricums hervorgerufene electrodynamische Kraft", *Ann. Phys.* 35(10): 264, 1888.
- [69] Dzyaloshinskii, I. E., “On the magneto-electrical effects in antiferromagnets”, *Sov. Phys. JETP*, 10, pp. 628-629, 1960.
- [70] Astrov, D. N., “The magnetoelectric effect in antiferromagnetic”, *Sov. Phys. JETP*, 11, pp. 708-709, 1960.
- [71] Astrov, D. N., “Magnetoelectric effect in chromium oxide”, *Sov. Phys. JETP*, 13, pp. 729-733, 1961.
- [72] Rado, G. T., Folen, V. J., “Observation of the magnetically induced magnetoelectric effect and evidence for antiferromagnetic domains”, *Phys. Rev. Lett.*, Vol. 7, pp. 310, 1961.
- [73] Folen, V. J., Rado, G. T., Stalder, E. W., “Anisotropy of the magnetoelectric effect in Cr_2O_3 ”, *Phys. Rev. Lett.*, Vol. 6, pp. 607, 1961.
- [74] Nan, C. W., Bichurin, M. I., Dong, S., Viehland, D., Srinivasan, G., "Multiferroic magnetoelectric composites: Historical perspective, status, and future directions". *J. Appl. Phys.*, Vol. 103 (3), pp. 031101-35, 2008.
- [75] Lawes, G., Ramirez, A. P., Varma, C. M., and Subramanian, M. A., “Magnetodielectric effects from spin fluctuations in isostructural ferromagnetic and antiferromagnetic systems”, *Phys. Rev. Lett.*, 91, 257208, 2003.
- [76] Solovyev, I. V., Pchelkina, Z. V., “Orbital ordering and magnetic interactions in BiMnO_3 ”, *New J. Phys.*, Vol. 10, pp. 073021, 2008.
- [77] Wang, J., Neaton, J. B., Zheng, H., Nagarajan, V., Ogale, S. B., Liu, B., Viehland, D., Vaithyanathan, V., Schlom, D. G., Waghmare, U. V., Spaldin, N. A., Rabe, K. M., Wuttig, M., Ramesh, R., “Epitaxial BiFeO_3 multiferroic thin film heterostructures”, *Science*, Vol. 299, pp. 1719, 2003.
- [78] Hur, N., Park, S.; Sharma, P. A.; Ahn, J. S.; Guha, S.; Cheong, S. W., “Electric polarization reversal and memory in a multiferroic material induced by magnetic fields”, *Nature*, Vol. 429, 392, 2004.
- [79] Goodenough, J. B., “Theory of the role of covalence in the perovskite-type manganites $[\text{La}, \text{M}(\text{II})]\text{MnO}_3$ ”, *Phys. Rev.*, Vol. 100, pp. 564-573, 1955.

- [80] Miller, J. S., "Organic- and molecule-based magnets", *Pramana - J. Phys.*, Vol. 67, No.1, pp. 1-16, 2006.
- [81] Morrish, A. H., "The physical principles of magnetism", *Wiley, New York*, 1965.
- [82] Spaldin, N. A., "Magnetic materials - fundamentals and applications", *Cambridge University Press, New York*, 2010.
- [83] Darezereshki, E., Bakhtiari, F., Alizadeh, M. and Ranjbar, M., "Direct thermal decomposition synthesis and characterization of hematite (α -Fe₂O₃) nanoparticles", *Mater. Sci. Semicond. Process.*, Vol. 15, pp. 91-97, 2012.
- [84] Nelson, S. O., and Datta, A. K., "Dielectric properties of food materials and electric field interactions", *Handbook of microwave technology for food application*, CRC Press, pp. 93-138, 2001.
- [85] Nelson, S. O., "Electrical properties of agricultural products – A critical review", *Trans. ASAE*, Vol. 16(2), pp. 384-400, 1973.
- [86] Nelson, S. O., "Dielectric properties of agricultural products - measurements and applications", *IEEE Trans. Electr. Insul.*, 26(5), pp. 845-869, 1991.
- [87] Debye, P., "Polar molecules, New York, The Chemical Catalog Co.", 1929.
- [88] Sebastian, M. T., "Dielectric materials for wireless communication", *Elsevier*, 2010.
- [89] Wahab, M. A., *Solid state physics: structure and properties of materials*, Alpha Science Int'l Ltd., 2005.
- [90] Kittel, C., McEuen, P., *Introduction to solid state physics*, New York: Wiley, Vol. 8, 1996.
- [91] Rao, K. H., Raju, S. B., Aggarwal, K., and Mendiratta, R. G., "Effect of Cr impurity on the dc resistivity of Mn-Zn ferrites", *J. Appl. Phys.*, Vol. 52, pp. 1376, 1981.
- [92] Callegaro, L., "Electrical impedance: principles, measurement, and applications", CRC Press, 2012.
- [93] Lacerda, L. H. S., Ribeiro, R. A. P., and Lazaro, S. R., "Magnetic, electronic, ferroelectric, structural and topological analysis of AlFeO₃, FeAlO₃, FeVO₃, BiFeO₃ and PbFeO₃ materials: Theoretical evidence of magnetoelectric coupling", *J. Magn. Magn. Mater.*, 2019.
- [94] Feng, H., "Magnetism and electronic properties of BiFeO₃ under lower pressure", *J. Magn. Magn. Mater.*, Vol. 322, pp. 3755-3759, 2010.

- [95] Je-Geun, P., Duc, L. M., Jaehong, J., Sanghyun, L., “Structure and spin dynamics of multiferroic BiFeO₃”, *J. Phys.: Condens. Matter*, Vol. 26, pp. 433202, 2014.
- [96] We, J. H., Kim, S. J., and Kim, C. S., “Magnetic properties on ferromagnetic FeAlO₃”, *IEEE Tran. Mag.*, Vol. 42, pp. 2876-2878, 2006.
- [97] Saha, R., Shireen, A., Bera, A. K., Shirodkar, S. N., Sundarayya, Y., Kalarikkal, N., Yusuf, S. M., Waghmare, U. V., Sundaresan, A., Rao, C. N. R., “Structure and magnetic properties of the Al_{1-x}Ga_xFeO₃ family of oxides: A combined experimental and theoretical study”, *J. Solid State Chem.*, Vol. 184, pp. 494–501, 2011.
- [98] X. Devaux, A. Rousset, J. M. Broto, H. Rakoto, and S. Askenazy, “FeAlO₃: new production methods and study of its magnetization in very high intensity pulsed magnetic fields”, *J. Mater. Sci. Lett.*, Vol. 9, pp. 371-372, 1990.
- [99] Cross, L. E., “Relaxor ferroelectrics”, *Ferroelectrics*, Vol. 76, 241-267, 1987.
- [100] Cótica, L. F., Santos, G. M., Freitas, V. F., Coelho, A. A., Pal, M., Santos, I. A., Garcia, D., Eiras, J. A., Guo, R., and Bhalla, A. S., “Room temperature nonlinear magnetoelectric effect in lead-free and Nb-doped AlFeO₃ compositions”, *J. Appl. Phys.*, Vol. 117, pp. 064104-(1-7), 2015.
- [101] Caracas, R., “Spin and structural transitions in AlFeO₃ and FeAlO₃ perovskite and post-perovskite”, *Phys. Earth Planet. Inter.*, Vol. 182, pp. 10-17, 2010.
- [102] Levy, M. R., “Crystal structure and defect property predictions in ceramic materials”, Ph.D. diss., *University of London*, 2005.
- [103] Mackenzie, K. J. D., Brown, I. W. M., “The Mössbauer spectrum and structure of iron(III) aluminium oxide, FeAlO₃”, *J. Mater. Sci. Lett.*, Vol. 3, pp. 159, 1984.
- [104] Villafuerte-Castrejon, M. E., Castillo-Pereyra, E., tartaj, J., Fuentes, L., Bueno-Baques, D., Gonzalez, G., Matutes-Aquino, J. A., “Synthesis and AC magnetic susceptibility measurements of Fe_(2-x)Al_xO₃ compounds”, *J. Magn. Magn. Mater.*, Vol. 837, pp. 272-276, 2004.
- [105] Bruno, G., Efremov, A. M., Clausen, B., Balagurov, A. M., Simkin, V. N., Wheaton, B. R., Webb, J.E., Brown, D. W., “On the stress-free lattice expansion of porous cordierite”, *Acta Mater.*, Vol. 58, pp. 1994-2003, 2010.
- [106] Shannon, R. D., “Revised effective ionic radii and systematic studies of interatomic distances in halides and chalcogenides”, *Acta Cryst.*, A 32, 751-767, 1976.
- [107] Singh, S. K., and Ishiwara, H., “Room-temperature ferroelectric properties of Mn-substituted BiFeO₃ thin films deposited on Pt electrodes using chemical solution deposition,” *Appl. Phys. Lett.*, vol. 88, no. 26, Article ID 262908, 2006.
- [108] Mukherjee, A., Basu, S., Green, L. A. W., Thanh, N. T. K., Pal, M., “Enhanced

- multiferroic properties of Y and Mn codoped multiferroic BiFeO₃ nanoparticles”, *J. Mater. Sci.*, Vol. 50, pp. 1891–1900, 2015.
- [109] Thomas, E., Sippel, P., Reuter, D., Weiß, M., Loidl, A. and Krohns, S., “Dielectric study on mixtures of ionic liquids”, *Sci. Rep.* 7, Article number: 7463, 2017.
- [110] Belkin, A., Bezryadin, A., Hendren, L., and Hubler, A., “Recovery of Alumina nano capacitors after high voltage breakdown”, *Sci. Rep.*, 7(1), pp. 1-7, 2017.
- [111] Crangle, J. and Goodman, G. M., “The magnetization of pure iron and nickel”, *Proceedings of the Royal Society of London. Series A, Math. Phys. Sci.*, Vol. 321, No. 1547, pp. 477-491, 1971.
- [112] Ling, P., Minhong, J., Zhengfei, G., Gang, C., Lei, M., Yusong, D., Xiaofei, W., Guanghui, R., and Yongxiang, L., “Structure and piezoelectric properties of K_{0.5}Na_{0.5}NbO₃–AlFeO₃ lead-free ceramics by using AlFeO₃ as a sintering aid”, *J. Mater. Sci.: Mater Electron*, Vol. 25, pp. 323–327, 2014.
- [113] Galarrage, C. E., “Heterogeneous catalyst for the synthesis of middle distillate hydrocarbons”, M.S. thesis, University of Western Ontario, London, Canada, 1998.
- [114] Rečko, K., Waliszewski, J., Klekotka, U., Soloviov, D., Ostapczuk, G., Satuła, D., Biernacka, M., Balasoju, M., Basa, A., Kalska-Szostko, B., and Szymański, K., “Phase composition and magnetism of sol–gel synthesized Ga–Fe–O nanograins”, *Phase Transitions*, pp. 1-12, 2017.
- [115] Fiebig, M., Lottermoser, T. H., Fröhlich, D., Goltsev, A. V. and Pisarev, R. V., “Observation of coupled magnetic and electric domains”, *Nature*, Vol. 419, pp. 818 -820, 2002.
- [116] M. Anis-ur-Rehman, G. Asghar, “Variation in structural and dielectric properties of co-precipitated nanoparticles Strontium ferrites due to value of pH”, *J. Alloys Compd.*, Vol. 509, pp. 435-439, 2011.
- [117] Koops, C. G., “On the dispersion of resistivity and dielectric constant of some semiconductors at audio frequencies”, *Phys. Rev.*, Vol. 83, pp. 121-124, 1951.
- [118] Rezlescu, N., and Rezlescu, E., “Dielectric properties of copper-containing ferrites”, *Phys. Stat. Sol. A.*, Vol. 23, pp. 575-582, 1974.
- [119] Sun, K., Fan, R., Yin, Y., Guo, J., Li, X. F., Lei, Y., An, L., Cheng, C., Guo, Z., “Tunable negative permittivity with fano-like resonance and magnetic property in percolative Silver/Yttrium Iron garnet nanocomposites”, *J. Phys. Chem. C*, 7564-7571, 2017.
- [120] Fouskova, A. and Cross, L. E., “Dielectric properties of Bismuth Titanate”, *J. Appl. Phys.*, Vol. 41, pp. 2834, 1970.

- [121] Dutta, A., and Sinha, T. P., “Dielectric relaxation and electronic structure of $\text{Ca}(\text{Fe}_{1/2}\text{Sb}_{1/2})\text{O}_3$ ”, *Phys. Rev. B*, Vol. 76, pp. 155113, 2007.
- [122] Mohamed, M. B., Wang, H., and Fuess, H., “Dielectric relaxation and magnetic properties of Cr doped GaFeO_3 ”, *J Phys. D: Appl. Phys.*, Vol. 43, pp. 455409, 2010.
- [123] Bauerle, E., “Study of solid electrolyte polarization by a complex admittance method”, *J. Phys. Chem.*, Vol. 30, pp. 2657-2670, 1969.
- [124] Macdonal J. R., Johnson W. B., “Fundamentals of impedance spectroscopy”, Wiley, Hoboken, 2005.
- [125] Kumari, K., Prasad, A., Prasad, K., “Dielectric, impedance/modulus and conductivity studies on $[\text{Bi}_{0.5}(\text{Na}_{1-x}\text{K}_x)_{0.5}]_{0.94}\text{Ba}_{0.06}\text{TiO}_3$, ($0.16 \leq x \leq 0.20$) Lead-free ceramics”, *Am. J. Mater. Sci.*, Vol. 6(1), pp. 1-18, 2016.
- [126] Mathur, P., Thakur, A., Singh, M., “Study of low temperature sintered nanocrystalline Mn-Cu-Zn ferrite prepared by coprecipitation method”, *Mod Phys. Lett.*, Vol. 21, pp. 1425 – 1430, 2007.
- [127] Akhter, S., Paul, D. P., Hakim, M. A., Akhter, S., Saha, D. K., Anjuman, B., and Islam, F., “Microstructure and complex permeability spectra of polycrystalline Cu-Zn Ferrites”, *J. Sci. Res.*, Vol. 4 (3), pp. 551-560, 2012.
- [128] Ahsan, M. Z., Khan, F. A., Islam, M. A., Tabassum, T., Alam, M. K., “Study on AC permeability and permittivity of manganese doped cobalt ferrite nanoparticles”, *J. Phys. Commun.*, Vol. 2, pp. 105008:1 – 6, 2018.
- [129] Ahsan, M. Z., Khan, F. A., “Structural and electrical properties of manganese doped cobalt ferrite nanoparticles”, *Mater Sci. Nanotechnol.*, Vol. 2, pp. 1-9, 2018.
- [130] A. Ahad, M. A. Taher, Mithun Kumar Das, M. Zahidur Rahaman, M. N. I. Khan, “Effect of Y substitution on magnetic and transport properties of $\text{Ba}_{0.95}\text{La}_{0.05}\text{Ti}_{1-x}\text{Y}_x\text{O}_3$ ceramics”, *Results Phys.*, Vol. 12, pp. 1925 – 1932, 2019.
- [131] Maaz, K., Mumtaz, A., Hasanian, S. K., Ceylon, A., “Synthesis and magnetic properties of cobalt ferrite (CoFe_2O_4) nanoparticles prepared by wet chemical route”, *J. Magn. Magn. Mater.*, Vol. 308(2), pp 389-395, 2007.
- [132] Zhu, X. H., Zhu, J. M., Zhou, S. H., Liu, Z. G., Ming, N. B., and Hesse D., “Microstructural characterization of BaTiO_3 ceramic nanoparticles synthesized by the Hydrothermal technique”, *Solid State phenomena*, Vol. 106, pp. 41–46, 2005.
- [133] Ahsan, M. Z., Islam, A., Bally, A. A., Khan, F. A., “Spectroscopic analysis for electric and magnetic properties of manganese doped cobalt nano ferrite”, *Results Phys.*, Vol. 17, pp. 103172, 2020.

Appendix

List of Presentation

1. T. Tabassum, M. Z. Ahsan, M. K. Alam, and F. A. Khan, “ Structural, Electrical and Magnetic Properties of Mn Doped AlFeO_3 ”, presented at *Natl. Conf. on Electronics and Informatics*, Atomic Energy Centre, Dhaka, MS (II)-06, pp. 72, 2019.

